
Exponential-Family Membership Inference: From LiRA and RMIA to BaVarIA

Rickard Brännvall¹

¹RISE Research Institutes of Sweden

Abstract

Membership inference attacks (MIAs) are becoming standard tools for auditing the privacy of machine learning models. The leading attacks—LiRA [Carlini et al., 2022] and RMIA [Zarifzadeh et al., 2024]—appear to use distinct scoring strategies, while the recently proposed BASE [Lassila et al., 2025] was shown to be equivalent to RMIA, making it difficult for practitioners to choose among them. We show that all three are instances of a single exponential-family log-likelihood ratio framework, differing only in their distributional assumptions and the number of parameters estimated per data point. This unification reveals a hierarchy (BASE1–4) that connects RMIA and LiRA as endpoints of a spectrum of increasing model complexity. Within this framework, we identify variance estimation as the key bottleneck at small shadow-model budgets and propose BaVarIA, a Bayesian variance inference attack that replaces threshold-based parameter switching with conjugate normal-inverse-gamma priors. BaVarIA yields a Student- t predictive (BaVarIA- t) or a Gaussian with stabilized variance (BaVarIA- n), providing stable performance without additional hyperparameter tuning. Across 12 datasets and 7 shadow-model budgets, BaVarIA matches or improves upon LiRA and RMIA, with the largest gains in the practically important low-shadow-model and offline regimes.

1 INTRODUCTION

Membership inference attacks (MIAs) determine whether a specific data point was used to train a machine learning model [Shokri et al., 2017]. Beyond their role as privacy attacks, MIAs serve as empirical auditing tools: they provide lower bounds on the privacy leakage of trained models [Nasr

et al., 2023, Steinke et al., 2023], complementing theoretical guarantees from differential privacy [Dwork et al., 2006]. As with any auditing technique, the same methods could in principle be misused; we focus on the defensive application throughout.

The current landscape of score-based MIAs presents practitioners with several competing approaches. LiRA [Carlini et al., 2022] fits per-point Gaussian models to shadow-model log-odds and computes a likelihood-ratio score. RMIA [Zarifzadeh et al., 2024] uses a population-level reference to avoid per-point parameter estimation. BASE [Lassila et al., 2025] centers the target loss against a pooled shadow summary. Lassila et al. [2025] proved that BASE and RMIA are equivalent, but the connection between these population-level methods and LiRA’s per-point Gaussian approach has not been established.

We clarify the relationship by showing that LiRA, RMIA, and BASE are all instances of a single framework. The key insight is that each attack implicitly assumes a parametric distribution for a scalar summary statistic (loss, confidence, or log-odds) under the IN and OUT membership hypotheses, and then computes the corresponding log-likelihood ratio (LLR). Different distributional assumptions and parameter-sharing constraints yield different attacks.

This unification yields three contributions:

(1) A unifying framework (Section 3). We formalize the exponential-family LLR and show that it specializes to known attacks under specific distributional assumptions (Exponential, Gaussian). We define the BASE hierarchy (BASE1–4), a family of Gaussian LLR attacks with progressively relaxed parameter sharing, connecting RMIA/BASE at one end to LiRA at the other.

(2) BaVarIA: Bayesian Variance Inference Attack (Section 4). LiRA’s performance degrades at small shadow-model budgets K because per-point variance estimates become unreliable. We replace maximum likelihood estimation with conjugate normal-inverse-gamma (NIG) Bayesian

inference, yielding two variants: BaVarIA- t (Student- t predictive) and BaVarIA- n (Gaussian with Bayesian variance). Both provide Bayesian shrinkage that smoothly transitions from global to per-point estimates as K grows, with all posterior updates available in closed form.

(3) Empirical evaluation (Section 5). We evaluate all methods across 12 datasets (image and tabular), 7 shadow-model budgets ($K \in \{4, \dots, 254\}$), and 32 experimental replicates. On average, BaVarIA- n matches or improves over LiRA at $K \geq 16$, while BaVarIA- t provides the best AUC across all K . We validate findings on an independent shadow-model collection.

2 BACKGROUND

Setup. Let $D = \{(x_i, y_i)\}_{i=1}^N$ be a dataset. A target model $f(\cdot; \theta_0)$ is trained on a subset $S_0 \subset D$, and K shadow models $f(\cdot; \theta_k)$, $k = 1, \dots, K$, are each trained on subsets $S_k \subset D$. For a fixed point i , the membership indicator $m_{i,k} \in \{0, 1\}$ records whether $(x_i, y_i) \in S_k$. Membership is known for shadows ($k > 0$) and unknown for the target ($k = 0$).

We observe the per-point loss $\ell_{i,k} = \ell(f(x_i; \theta_k), y_i)$, the predicted confidence $p_{i,k}$ for the true label, and form scalar statistics such as the rescaled logit $\varphi_{i,k} = \log(p_{i,k}/(1 - p_{i,k}))$. Under cross-entropy loss, $\ell = -\log p$, so all three quantities are monotone transforms of the same signal.

Optimal membership score. Sablayrolles et al. [2019] showed that the Bayes-optimal membership score is the log-likelihood ratio

$$\text{LLR}(z) = \log \frac{p(z \mid m = 1)}{p(z \mid m = 0)}, \quad (1)$$

where z is any sufficient scalar statistic of the model output. Their analysis further shows that the optimal attack depends on the model only through the loss, so black-box access to a scalar output statistic is sufficient—justifying the restriction to scalar statistics throughout this paper. All score-based MIAs can be viewed as estimating this quantity under different modeling assumptions.

LiRA. For each point i , LiRA [Carlini et al., 2022] models the rescaled logit $\varphi_{i,k} \mid m = m' \sim \mathcal{N}(\mu_{i,m'}, \sigma_{i,m'}^2)$ with parameters estimated from shadow models. Let $\mathcal{K}_{i,m} = \{k > 0 : m_{i,k} = m\}$. The LiRA score is

$$\text{LiRA}_i = \frac{(\varphi_{i,0} - \hat{\mu}_{i,0})^2}{2\hat{\sigma}_{i,0}^2} - \frac{(\varphi_{i,0} - \hat{\mu}_{i,1})^2}{2\hat{\sigma}_{i,1}^2} + \log \frac{\hat{\sigma}_{i,0}}{\hat{\sigma}_{i,1}}, \quad (2)$$

where $\hat{\mu}_{i,m}$ and $\hat{\sigma}_{i,m}^2$ are the MLE from $\{\varphi_{i,k}\}_{k \in \mathcal{K}_{i,m}}$.

RMIA and BASE. RMIA [Zarifzadeh et al., 2024] computes a likelihood ratio against a population reference, avoiding per-point parameter estimation. BASE [Lassila et al.,

2025] scores each point by centering the target loss against a pooled shadow summary:

$$\text{BASE}_i = -\ell_{i,0} - \log\left(\frac{1}{K} \sum_{k=1}^K e^{-\ell_{i,k}}\right). \quad (3)$$

Lassila et al. [2025] proved that BASE and RMIA (at $\gamma = 1$) produce equivalent ROC curves.

3 EXPONENTIAL-FAMILY FRAMEWORK

We now show that the attacks of Section 2 are instances of a single parametric framework. For a fixed point i , assume the scalar statistic $z_{i,k} \mid m_{i,k} = m$ follows an exponential-family distribution

$$p(z \mid m) = h(z) \exp(\eta_m^\top T(z) - A(\eta_m)), \quad (4)$$

with sufficient statistics $T(z)$, natural parameters η_m , base measure $h(z)$, and log-partition function A . The LLR (1) then takes the form

$$\text{LLR}(z) = (\eta_1 - \eta_0)^\top T(z) - (A(\eta_1) - A(\eta_0)), \quad (5)$$

which is an affine function of $T(z)$. Under any exponential-family model, the optimal membership score is thus a linear combination of the sufficient statistics, plus a constant offset.

3.1 DISTRIBUTIONAL SPECIALIZATIONS

We consider two primary distributional families; others (Beta, Gamma) are developed in Appendix A.

Exponential model (loss statistic). Assume $\ell_{i,k} \mid m \sim \text{Exp}(\lambda_m)$. The LLR is

$$\text{LLR}(\ell) = \log \frac{\lambda_1}{\lambda_0} - (\lambda_1 - \lambda_0) \ell, \quad (6)$$

which is linear in the target loss without any structural constraint—the one-parameter exponential family yields an affine LLR automatically.

Gaussian model (log-odds statistic). Assume $\varphi_{i,k} \mid m \sim \mathcal{N}(\mu_m, \sigma_m^2)$. The LLR is

$$\text{LLR}(\varphi) = \frac{(\varphi - \mu_0)^2}{2\sigma_0^2} - \frac{(\varphi - \mu_1)^2}{2\sigma_1^2} + \log \frac{\sigma_0}{\sigma_1}. \quad (7)$$

Under equal variances $\sigma_0^2 = \sigma_1^2 = \sigma^2$, this reduces to

$$\text{LLR}(\varphi) = \frac{\mu_1 - \mu_0}{\sigma^2} \left(\varphi - \frac{\mu_1 + \mu_0}{2} \right), \quad (8)$$

which is linear in φ .

Table 1 summarizes the distributional families and their LLR forms.

Table 1: Exponential-Family LLR-Based Attacks.

Model	Statistic z	Params	LLR form
Exponential	loss ℓ	2	linear in ℓ
Gaussian	log-odds φ	4	φ, φ^2
(equal var.)	log-odds φ	3	linear in φ
<i>Additional families (Appendix A):</i>			
Gamma	loss ℓ	4	$\ell, \log \ell$
Beta	confidence p	4	$\log p, \log(1-p)$

3.2 THE BASE HIERARCHY

We define a hierarchy of four attacks by progressively relaxing parameter-sharing constraints. BASE1–4 follow from the Gaussian LLR (7) under decreasing levels of parameter sharing; BASE1 can also be derived from any one-parameter exponential family, including the exponential (6), and Gamma models (Appendix B). All variants operate on a scalar statistic $z_{i,k}$ (loss, log-odds, or confidence) and differ only in how parameters are estimated from shadow models. The derivation chain and two formal corollaries (LiRA = BASE4, BASE = BASE1) are given in Appendix B; here we summarize.

BASE1 (pooled centering). Under a constant LLR slope, only the per-point centering affects the ranking; pooling all shadows to estimate this center gives:

$$\text{BASE1}_i = z_{i,0} - \hat{z}_{i,\text{pool}}, \quad (9)$$

where $\hat{z}_{i,\text{pool}}$ is estimated from all K shadows. Setting $z = -\ell$ with log-sum-exp centering recovers the BASE score (3); the same result follows independently from the exponential and Gamma models (Appendix B).

BASE2 (pooled centering and variance). Under the Gaussian model with equal variance and a constant mean gap $\mu_{i,1} - \mu_{i,0} = \Delta\mu$, the LLR is

$$\text{BASE2}_i = (z_{i,0} - \hat{\mu}_{i,\text{pool}}) / \hat{\sigma}_i^2, \quad (10)$$

where $\hat{\mu}_{i,\text{pool}}$ and $\hat{\sigma}_i^2$ are estimated from all shadows.

BASE3 (separate means, pooled variance). Relaxing the constant-gap assumption, we estimate means separately for IN and OUT shadows while pooling variance:

$$\text{BASE3}_i = \frac{\hat{\mu}_{i,1} - \hat{\mu}_{i,0}}{\hat{\sigma}_i^2} \left(z_{i,0} - \frac{\hat{\mu}_{i,1} + \hat{\mu}_{i,0}}{2} \right). \quad (11)$$

BASE4 (class-conditional parameters). Removing all parameter-sharing constraints and substituting MLE into the Gaussian LLR (7) gives four per-point parameters $(\hat{\mu}_{i,m}, \hat{\sigma}_{i,m}^2)$ for $m \in \{0, 1\}$:

$$\text{BASE4}_i = \frac{(\varphi_{i,0} - \hat{\mu}_{i,0})^2}{2\hat{\sigma}_{i,0}^2} - \frac{(\varphi_{i,0} - \hat{\mu}_{i,1})^2}{2\hat{\sigma}_{i,1}^2} + \log \frac{\hat{\sigma}_{i,0}}{\hat{\sigma}_{i,1}}. \quad (12)$$

Proposition 1 (Equivalences). *Under the standard implementations: (a) BASE1 on loss with log-sum-exp centering is ROC-equivalent to RMIA at $\gamma = 1$; (b) BASE4 on rescaled logits coincides with LiRA (2).*

Part (a): Lassila et al. [2025] proved that the original BASE score (3) is ROC-equivalent to RMIA; Corollary 2 in the appendix shows that BASE is an instance of BASE1. Part (b) follows from substituting MLE into the Gaussian LLR (7) (Corollary 1).

The hierarchy BASE1 \rightarrow BASE2 \rightarrow BASE3 \rightarrow BASE4 thus connects RMIA and LiRA as endpoints of a spectrum of increasing model complexity. Moving from BASE1 to BASE4 trades robustness for expressiveness: BASE1 estimates no per-point dispersion parameters (maximally pooled), while BASE4 estimates four per-point parameters (maximally flexible). The intermediate variants BASE2 and BASE3 offer controlled intermediate points; empirically, BASE3 is competitive with BASE4 at moderate K (Section 5).

3.3 WHEN DOES MORE STRUCTURE HELP?

The hierarchy reveals a bias-variance tradeoff in the estimation of the LLR. RMIA/BASE does not require an explicit distributional assumption in its original formulation; we show that it is equivalent to an exponential model with a pooled mean estimate. LiRA/BASE4 models the full Gaussian with separate parameters per class, exploiting variance differences that carry strong membership signal, but requiring enough data to estimate all four parameters reliably.

This tradeoff predicts that LiRA should dominate RMIA when K is large enough for per-point Gaussian estimation, while RMIA should be preferable at very small K where Gaussian parameters are poorly estimated.

4 BAVARIA: BAYESIAN VARIANCE INFERENCE ATTACK

The framework of Section 3 shows that LiRA is a Gaussian plug-in LLR with per-point MLE parameters. When K is small, these estimates—especially the variance—become unreliable, motivating a Bayesian treatment.

4.1 THE SMALL- K PROBLEM

With K shadow models and balanced membership, each point has approximately $K/2$ IN and $K/2$ OUT observations. At $K = 8$, per-class variance is estimated from ~ 4 samples—insufficient for reliable estimation. Carlini et al. [2022] address this with a hard switch: when fewer than ~ 32 observations are available per class (i.e., $K < 64$ total shadow models), per-point variances are replaced by a single global variance computed across all points. This

approach has two limitations. First, it is discontinuous: the attack behavior changes abruptly at the threshold. Second, it is all-or-nothing: it cannot leverage partial information from small per-point samples while also incorporating global information. A natural alternative is to smoothly interpolate between global and per-point estimates based on the available evidence.

4.2 NIG PRIOR AND POSTERIOR PREDICTIVE

We place a normal-inverse-gamma (NIG) prior on the class-conditional parameters:

$$(\mu_m, \sigma^2) \sim \text{NIG}(\mu_{\emptyset, m}, \kappa_{\emptyset}, \alpha_{\emptyset}, \beta_{\emptyset, m}), \quad (13)$$

where subscript \emptyset denotes the prior—the hyperparameters before observing any point-specific data—estimated via empirical Bayes from pooled shadow statistics (details in Appendix C); the class-specific parameters $\mu_{\emptyset, m}$ and $\beta_{\emptyset, m}$ are estimated separately for each class m , while the strength parameters κ_{\emptyset} and α_{\emptyset} are shared. Given $n_m = |\mathcal{K}_{i, m}|$ shadow observations with sample mean \bar{z}_m and sum of squares S_m , the posterior is $\text{NIG}(\mu'_{i, m}, \kappa'_{i, m}, \alpha'_{i, m}, \beta'_{i, m})$ with standard conjugate updates

$$\begin{aligned} \mu'_{i, m} &= \frac{\kappa_{\emptyset} \mu_{\emptyset, m} + n_m \bar{z}_m}{\kappa_{\emptyset} + n_m} \\ \kappa'_{i, m} &= \kappa_{\emptyset} + n_m, \quad \alpha'_{i, m} = \alpha_{\emptyset} + \frac{n_m}{2}, \\ \beta'_{i, m} &= \beta_{\emptyset, m} + \frac{S_m}{2} + \frac{\kappa_{\emptyset} n_m (\bar{z}_m - \mu_{\emptyset, m})^2}{2(\kappa_{\emptyset} + n_m)} \end{aligned} \quad (14)$$

The posterior predictive for a new observation z under class m is a student t -distribution, $z | m \sim t(\nu_{i, m}, \tilde{\mu}_{i, m}, \tilde{\sigma}_{i, m}^2)$

$$\nu_{i, m} = 2\alpha'_{i, m}, \quad \tilde{\mu}_{i, m} = \mu'_{i, m}, \quad \tilde{\sigma}_{i, m}^2 = \frac{\beta'_{i, m} (\kappa'_{i, m} + 1)}{\alpha'_{i, m} \kappa'_{i, m}}. \quad (15)$$

4.3 TWO BAVARIA VARIANTS

BaVarIA- t (Student- t predictive). The LLR using the posterior-predictive Student- t densities is

$$\text{LLR}(z) = \log \frac{t_{\nu_{i, 1}} \left(\frac{z - \tilde{\mu}_{i, 1}}{\tilde{\sigma}_{i, 1}} \right)}{t_{\nu_{i, 0}} \left(\frac{z - \tilde{\mu}_{i, 0}}{\tilde{\sigma}_{i, 0}} \right)} - \log \frac{\tilde{\sigma}_{i, 1}}{\tilde{\sigma}_{i, 0}}, \quad (16)$$

where t_{ν} is the standard Student- t density with ν degrees of freedom. The heavier tails of the t -distribution absorb parameter uncertainty, providing stability in the small- K regime.

BaVarIA- n (Gaussian with Bayesian variance). To isolate the effect of better variance estimation from the heavier-tailed predictive, we define a hybrid variant: use MLE means

$\hat{\mu}_{i, m}$ (as in LiRA) but replace the MLE variance with the NIG posterior mean $\mathbb{E}[\sigma^2 | \text{data}] = \beta'_{i, m} / (\alpha'_{i, m} - 1)$, then compute the standard Gaussian LLR (7). This provides Bayesian shrinkage of the variance toward the global prior, serving as a continuous relaxation of the hard-switch strategy, while preserving the Gaussian LLR form.

5 EXPERIMENTS

5.1 SETUP

Datasets. We use 12 testbeds based on public datasets spanning image and tabular domains: 6 image (CIFAR-10/100 [Krizhevsky, 2009], CINIC-10 [Darlow et al., 2018], each with ResNet-18 [He et al., 2016] and WideResNet [Zagoruyko and Komodakis, 2016]) and 6 tabular (Location, Purchase100, Texas100, each with 3- and 4-layer MLPs).

Protocol. For each dataset, we train $K + 1$ models using the “Design B” protocol of Carlini et al. [2022]: one target model and K shadow models, each trained on a random half of the dataset. We evaluate at $K \in \{4, 8, 16, 32, 64, 128, 254\}$ and average over 32 replicates (rotated target).

Methods. We compare LiRA (= BASE4), RMIA (= BASE1), BASE3, BaVarIA- n , and BaVarIA- t .

Metrics. We report AUC and TPR at FPR = 0.01 (additional FPR thresholds in Appendix D).

5.2 MAIN RESULTS AT $K = 254$

Figure 1 shows log-log ROC curves for CIFAR-10 WideResNet at two shadow-model budgets. At $K = 8$ (left), RMIA leads on AUC because its pooled centering avoids the IN/OUT split that starves per-class estimation; BaVarIA- t is competitive while LiRA lags. At $K = 254$ (right), the Gaussian-family methods (LiRA, BaVarIA, BASE3) converge and outperform RMIA, confirming that richer distributional models benefit from adequate estimation budgets.

Table 2 reports the difference (Δ) relative to LiRA at the full shadow budget $K = 254$, averaged over 32 replicates; positive values indicate improvement over LiRA.

At $K = 254$, all methods have ample data for parameter estimation, so differences are small but informative. Three patterns emerge. First, RMIA (= BASE1) generally trails all Gaussian-family methods: the exponential model’s one-parameter structure does not model the variance differences between IN and OUT that the Gaussian model exploits. The gap is largest on CINIC-10 ResNet ($\Delta\text{AUC} = -0.081$) and Location ($\Delta\text{AUC} = -0.089$), datasets where the membership signal is concentrated in the tails of the log-odds distri-

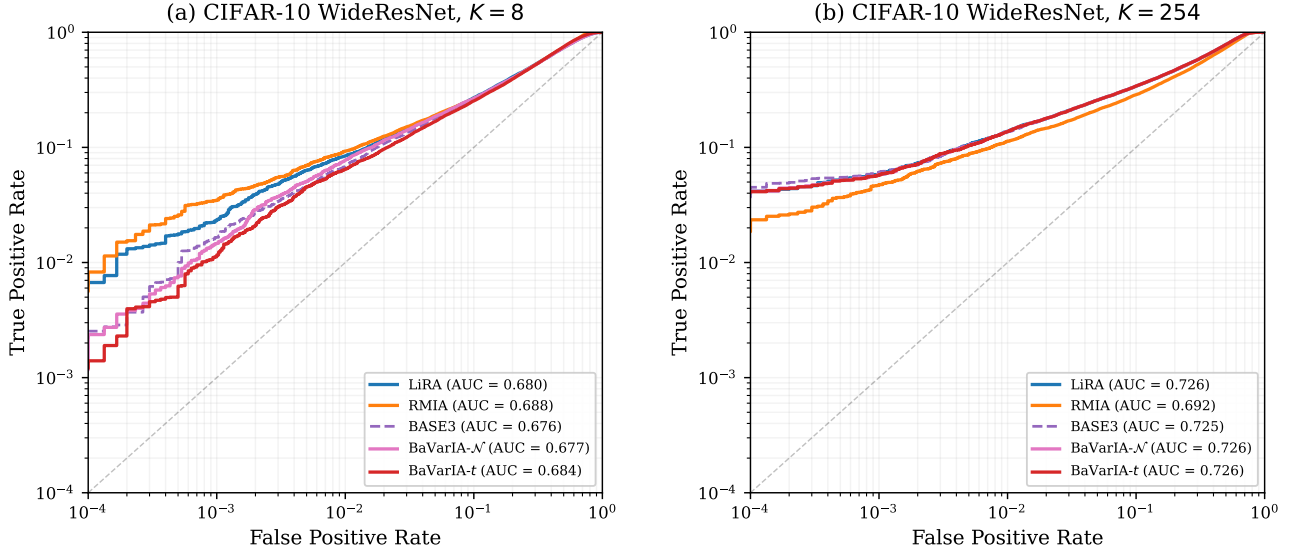


Figure 1: Log-log ROC curves for CIFAR-10 WideResNet at $K = 8$ (left) and $K = 254$ (right). At small K , RMIA’s pooled approach is competitive; at large K , the Gaussian-family methods dominate. BaVarIA- t bridges the gap, performing well across both regimes.

bution. Second, BASE3 (pooled variance, separate means) trails LiRA by a small margin ($\Delta\text{AUC} \approx -0.002$ on average), suggesting that separate variance estimation provides a slight benefit at large K , though the effect is small and not uniform across datasets. However, on tabular datasets like Purchase and Location, BASE3 occasionally matches or exceeds LiRA—pooled variance estimation is more stable when the mean separation is the dominant signal. Third, both BaVarIA variants match or marginally improve upon LiRA, with BaVarIA- t showing consistently non-negative ΔAUC across all 12 datasets, confirming it as a safe default at large K .

The same patterns are amplified for TPR@0.01 (Table 2, right columns). RMIA’s deficit grows to $\Delta\text{TPR} = -0.086$ on average, reaching -0.247 on CIFAR-100 ResNet—consistent with the prediction that its lack of variance modeling is most costly in the tails. BASE3 trails LiRA by 0.007 on average, and BaVarIA again matches LiRA, with all $|\Delta\text{TPR}| \leq 0.003$.

5.3 SCALING WITH SHADOW-MODEL BUDGET

Figure 2 shows performance as a function of K , averaged over image and tabular datasets. The advantage of BaVarIA over LiRA is largest in the small- K regime ($K \leq 16$), which is the most practically relevant since shadow models are expensive to train. Key observations across three regimes:

Small K (≤ 16). BaVarIA- t clearly separates from LiRA on AUC, with $\Delta\text{AUC} \approx +0.009$ at $K = 4$ averaged over 12 datasets. BaVarIA- n tracks LiRA more closely on TPR@0.01, making it the safer choice for low-FPR audit-

ing. RMIA is competitive with LiRA at $K = 4$: its pooled centering requires no IN/OUT split, which is advantageous when each class has only ~ 2 observations. This is consistent with the framework’s prediction: simpler models (fewer parameters per point) are preferable when estimation budgets are small (the SE bands in Figure 2 separate clearly at $K \leq 16$).

Medium K (32–64). LiRA’s MLE converges and the gap to BaVarIA narrows. BaVarIA- n still provides consistent small gains on TPR@0.01 ($\Delta \approx +0.017$ at $K = 32$), reflecting the continued value of Bayesian variance shrinkage. The gap narrows non-monotonically: BaVarIA’s advantage peaks at $K = 32$ and drops sharply at $K = 64$, precisely where LiRA’s hard switch activates per-point variance estimation (visible in the per-dataset scaling curves, Appendix D). BaVarIA’s smooth Bayesian interpolation avoids this discontinuity, yielding a monotonically improving scaling curve. RMIA plateaus relative to the Gaussian methods: at $K = 64$, TPR@0.01 averages 0.19 for RMIA vs. 0.27 for LiRA across all datasets (non-overlapping SE bands in Figure 2).

Large K (≥ 128). All Gaussian-family methods converge as the NIG posterior concentrates around the MLE. BaVarIA’s prior becomes non-informative and the Student- t degrees of freedom grow, so BaVarIA- $t \rightarrow$ BaVarIA- $n \rightarrow$ LiRA. The remaining method ordering (LiRA $>$ BASE3 $>$ RMIA) is stable and driven purely by structural differences in the LLR form.

Table 2: Performance Difference (Δ) vs. LiRA at $K = 254$ (32 Replicates). Positive Values Favor the Method.

Dataset	RMIA		BASE3		BaVarIA- n		BaVarIA- t	
	Δ AUC	Δ TPR _{.01}						
<i>Image datasets</i>								
C10-R18	+0.002	-0.002	+0.003	+0.001	+0.000	+0.000	+0.000	+0.000
C10-WRN	-.037	-0.029	-.001	-0.002	+0.000	+0.000	+0.000	+0.000
C100-R18	-.049	-0.247	-.004	-0.022	-.000	-0.000	+0.000	-0.000
C100-WRN	-.029	-0.056	-.002	-0.003	+0.000	+0.001	+0.000	+0.000
CN10-R18	-.081	-0.122	-.008	-0.013	+0.000	+0.000	+0.000	+0.000
CN10-WRN	-.054	-0.061	-.003	-0.004	-.000	+0.001	+0.000	+0.001
<i>Tabular datasets</i>								
Loc-3	-.072	-0.170	-.009	-0.030	+0.000	+0.001	+0.000	+0.001
Loc-4	-.089	-0.174	-.003	-0.002	+0.000	+0.002	+0.000	+0.003
Pur-3	-.002	-0.004	+0.002	+0.002	+0.000	+0.000	+0.000	+0.000
Pur-4	-.018	-0.017	+0.002	+0.002	+0.000	+0.001	+0.000	+0.001
Tex-3	-.025	-0.066	-.002	-0.007	+0.000	-0.000	+0.000	-0.000
Tex-4	-.038	-0.087	-.003	-0.006	-.000	+0.000	+0.000	+0.000
Average	-.041	-0.086	-.002	-0.007	+0.000	+0.000	+0.000	+0.001

5.4 BAVARIA ABLATION

Figure 3 isolates the two components of BaVarIA’s improvement. The ablation confirms that BaVarIA’s improvement decomposes into two separable effects: (1) *Better variance estimation* (BaVarIA- n): the NIG posterior mean shrinks noisy variance estimates toward a global prior, providing consistent improvement at $K \geq 16$ and gracefully converging to the MLE at large K . At $K = 32$, BaVarIA- n improves TPR@0.01 by +0.017 over LiRA on average—a substantial gain in the practically important regime. (2) *Heavier tails* (BaVarIA- t): the Student- t predictive improves AUC at all K (e.g., Δ AUC = +0.009 at $K = 4$) but hurts TPR at low FPR when K is small. At $K = 4$, the degrees of freedom $\nu \approx 6$ produce tails thick enough to increase false positives at extreme thresholds: Δ TPR@0.01 = -0.016 vs. LiRA, compared to +0.003 for BaVarIA- n . This reflects a ranking-precision tradeoff: the t -predictive accounts for parameter uncertainty, improving global ranking (AUC), but its heavier tails inflate scores for both members and non-members, increasing false positives at extreme thresholds.

The clean separation arises because BaVarIA- n uses the same Gaussian LLR as LiRA (isolating the variance estimation effect), while BaVarIA- t adds the Student- t predictive (adding the tail effect on top of better variance estimation).

5.5 DISTRIBUTIONAL DIAGNOSTICS

Per-datapoint Anderson-Darling tests (applied to each point’s ~ 128 IN and OUT shadow log-odds separately) reveal a range of departures from Gaussianity across datasets. On CIFAR-10 WideResNet, only $\sim 6\%$ of datapoints reject normality at the 5% level—close to the nominal rate—

indicating that per-datapoint Gaussianity is a good approximation. On CIFAR-100 ResNet, 74% of IN distributions reject normality, with heavy tails visible in the QQ plots (Appendix D.3). Despite these departures, the Gaussian-family methods (BASE3, BASE4/LiRA, BaVarIA) consistently dominate the alternatives across all datasets and metrics. This robustness is expected: the LLR score is evaluated at the *target* model’s output, which typically lies in the bulk of the distribution where the Gaussian approximation is accurate. These results suggest that moderate departures from Gaussianity do not preclude effective use of LiRA or BaVarIA in practice.

5.6 CROSS-VALIDATION

To verify that our findings generalize beyond a single training pipeline, we cross-validated all methods on an independent shadow-model collection trained without data augmentation or dropout (224–1,480 shadows per dataset). Models without augmentation exhibit substantially higher vulnerability on image datasets (e.g., CIFAR-10 ResNet AUC increases from 0.613 to 0.874), consistent with the known protective effect of data augmentation. However, the relative method ranking is fully preserved across both data sources: BaVarIA- $n \geq$ BaVarIA- $t \geq$ LiRA $>$ BASE3 $>$ RMIA $>$ BASE2. At $K = 64$ on the independent data, BaVarIA- n beats LiRA on TPR@0.01 in 10 of 12 datasets, with the exceptions being the two CIFAR-100 datasets where LiRA retains a marginal edge ($|\Delta$ TPR| $<$ 0.003). These findings hold across differences in training recipes and model regularization (Appendix G).

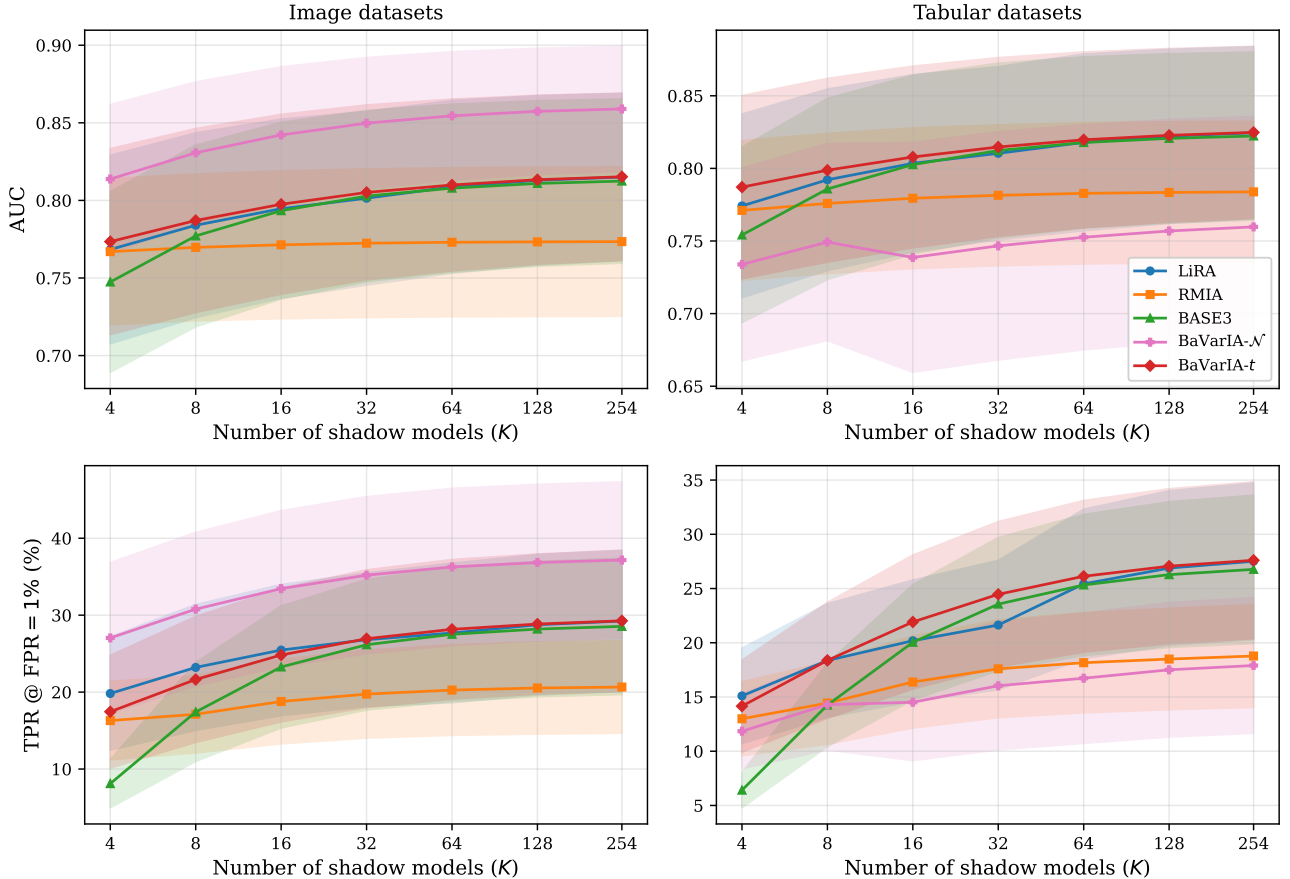


Figure 2: Performance vs. shadow-model budget K , averaged over 6 image datasets (left) and 6 tabular datasets (right). Top: AUC; Bottom: TPR@0.01. Shaded regions show ± 1 SE over 32 replicates. BaVarIA- t provides the best AUC at all K ; BaVarIA- n is safer at low FPR for small K .

5.7 OFFLINE SETTING

The framework extends naturally to the offline setting, where shadow data does not overlap with the target’s training set. BaVarIA is especially well-suited: with zero IN-class observations the NIG posterior reduces to the prior, recovering the behavior that LiRA’s variance switching achieves—but as a smooth limiting case requiring no separate implementation. Appendix I evaluates all methods offline across 12 datasets; no single method dominates, but offline performance remains viable for all approaches (Tables 12–13).

6 RELATED WORK

Membership inference attacks. MIA was introduced by Shokri et al. [2017], who trained binary classifiers on shadow-model outputs to distinguish members from non-members. Subsequent work simplified the attack surface: Yeom et al. [2018] showed that thresholding the loss suffices, and Sablayrolles et al. [2019] proved that the Bayes-optimal score is the log-likelihood ratio under IN vs. OUT,

deriving a global-threshold (MALT) to per-sample (MAST) approximation hierarchy. BaVarIA’s NIG prior interpolates smoothly along this axis, collapsing to a global prior (MALT-like) at small K and converging to per-point MLE (MAST-like) at large K . Carlini et al. [2022] operationalized this insight with LiRA, fitting per-point Gaussian models to shadow-model log-odds and achieving state-of-the-art results, albeit at the cost of many shadow models. Ye et al. [2022] and Watson et al. [2022] developed calibrated variants that account for difficulty heterogeneity across data points. Salem et al. [2019] demonstrated that relaxed threat models (fewer shadow models, different architectures) still yield effective attacks. More recently, Zarifzadeh et al. [2024] introduced RMIA, which compares the target output to a population reference rather than estimating per-point parameters, achieving competitive performance with lower computational cost. Lassila et al. [2025] introduced BASE in the context of MIA on graph neural networks, which simplifies for i.i.d. data to the conventional MIA setup, and proved that BASE and RMIA are ROC-equivalent, simplifying the landscape. Our framework unifies these approaches: LiRA, RMIA, and BASE are instances of exponential-

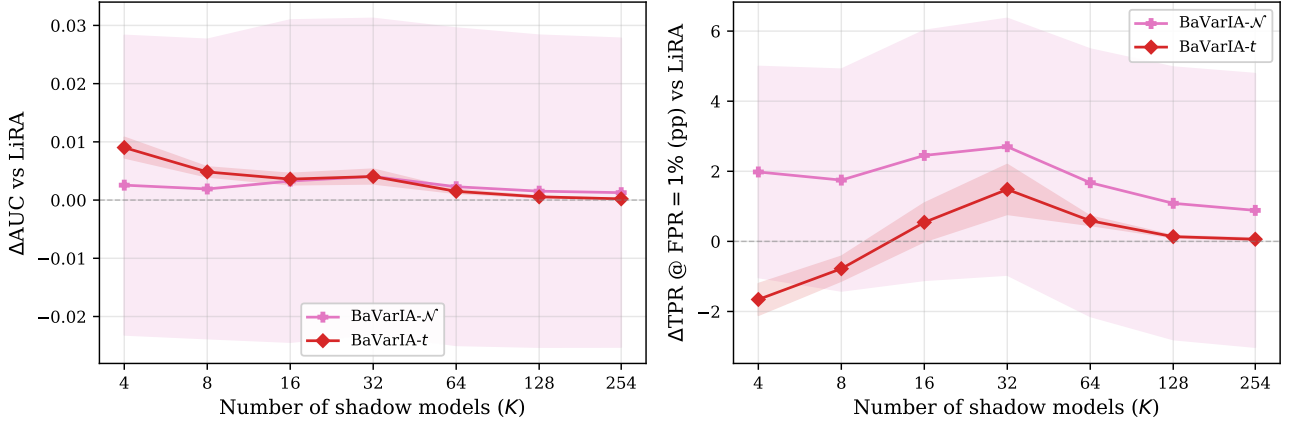


Figure 3: BaVarIA Ablation: Δ vs. LiRA Averaged over 12 Datasets. Left: AUC; Right: TPR@0.01. BaVarIA- t 's heavier tails help AUC uniformly but hurt TPR@0.01 at small K . BaVarIA- n provides safe improvement on both metrics at $K \geq 16$.

family LLR testing with different distributional assumptions and parameter-sharing constraints.

Privacy auditing. MIAs serve as empirical lower bounds on privacy leakage, complementing theoretical guarantees from differential privacy [Dwork et al., 2006]. Nasr et al. [2023] demonstrated that well-calibrated MIAs can produce tight auditing bounds that approach the theoretical (ϵ, δ) -DP guarantee. Steinke et al. [2023] showed that meaningful auditing is possible with only a single training run, reducing the computational burden. Song and Mittal [2021] provided a systematic evaluation framework for comparing MIA methods across diverse settings. Our work contributes to this line by providing practitioners with a method selection criterion based on the shadow-model budget K .

Bayesian methods and robust estimation. Conjugate Bayesian analysis of Gaussian parameters via normal-inverse-gamma priors is classical [Murphy, 2007, Gelman et al., 2013], and the resulting Student- t predictive is well understood. Shrinkage estimation [James and Stein, 1961] and empirical Bayes methods [Morris, 1983, Efron, 2010] provide principled frameworks for borrowing strength across related estimation problems. Our contribution applies this machinery to variance stabilization in membership inference: the NIG prior provides a shrinkage target that smoothly interpolates between global and per-point variance estimates as the sample size grows, replacing the hard switch of Carlini et al. [2022] with a continuous Bayesian alternative.

The exponential-family framework also accommodates Gamma and Beta distributional assumptions, and a discriminative extension (ELSA) that learns the LLR feature map; these are developed in Appendices E and H.

7 CONCLUSION

We presented an exponential-family framework that unifies the leading membership inference attacks—LiRA, RMIA, and the recently proposed BASE—as instances of log-likelihood ratio testing under different distributional assumptions. The resulting BASE hierarchy (BASE1–4) reveals these attacks as points on a spectrum from maximal pooling (RMIA/BASE) to full per-point estimation (LiRA/BASE4).

Within this framework, we identified variance estimation as the primary source of degradation at small K and proposed BaVarIA, which replaces LiRA's threshold-based variance switching with conjugate NIG Bayesian inference. The ablation of BaVarIA- n (Gaussian with Bayesian variance) and BaVarIA- t (Student- t predictive) cleanly separates the effects of better variance estimation from heavier-tailed predictives, providing practitioners with clear guidance: BaVarIA- n for low-FPR auditing, BaVarIA- t for general AUC.

Limitations. Our evaluation uses Design B resampling [Carlini et al., 2022] (each shadow model trains on a random half of the dataset; Section 5) with 32 replicates, which provides stable estimates for AUC and TPR@0.01 but limits precision for TPR@0.001. All methods assume access to shadow models trained on data from the same distribution; out-of-distribution transfer is not evaluated. The NIG hyperparameters are set via simple empirical Bayes defaults; more sophisticated hierarchical estimation could further improve small- K performance.

Practical recommendation. Use BaVarIA- n as a drop-in replacement for LiRA: it is rarely worse, and often better (especially at small K), requires no additional hyperparameter tuning, and runs in comparable time. For applications where AUC is the primary metric, BaVarIA- t provides a small additional improvement at all shadow budgets.

Future work. The exponential-family framework naturally extends to multi-output statistics (e.g., full softmax vectors rather than scalar confidence). The discriminative approach (ELSA, Appendix H) suggests that learning the LLR feature map from data—rather than fixing it via distributional assumptions—may yield further improvements when sufficient shadow models are available, particularly with automatic relevance determination for feature selection.

References

- Nicholas Carlini, Steve Chien, Milad Nasr, Shuang Song, Andreas Terzis, and Florian Tramèr. Membership inference attacks from first principles. In *IEEE Symposium on Security and Privacy (SP)*, pages 1897–1914. IEEE, 2022.
- Luke N Darlow, Elliot J Crowley, Antreas Antoniou, and Amos J Storkey. CINIC-10 is not ImageNet or CIFAR-10. *arXiv preprint arXiv:1810.03505*, 2018.
- Cynthia Dwork, Frank McSherry, Kobbi Nissim, and Adam Smith. Calibrating noise to sensitivity in private data analysis. In *Theory of Cryptography Conference (TCC)*, pages 265–284. Springer, 2006.
- Bradley Efron. *Large-Scale Inference: Empirical Bayes Methods for Estimation, Testing, and Prediction*. Cambridge University Press, 2010.
- Andrew Gelman, John B Carlin, Hal S Stern, David B Dunson, Aki Vehtari, and Donald B Rubin. *Bayesian Data Analysis*. CRC Press, 3rd edition, 2013.
- Kaiming He, Xiangyu Zhang, Shaoqing Ren, and Jian Sun. Deep residual learning for image recognition. In *IEEE Conference on Computer Vision and Pattern Recognition (CVPR)*, pages 770–778, 2016.
- William James and Charles Stein. Estimation with quadratic loss. *Proceedings of the Fourth Berkeley Symposium on Mathematical Statistics and Probability*, 1:361–379, 1961.
- Alex Krizhevsky. Learning multiple layers of features from tiny images. Technical report, University of Toronto, 2009.
- Marcus Lassila, Johan Östman, Khac-Hoang Ngo, and Alexandre Graell i Amat. Practical Bayes-optimal membership inference attacks. *arXiv preprint arXiv:2505.24089*, 2025.
- Carl N Morris. Parametric empirical Bayes inference: Theory and applications. *Journal of the American Statistical Association*, 78(381):47–55, 1983.
- Kevin P Murphy. Conjugate Bayesian analysis of the Gaussian distribution. *Technical report, University of British Columbia*, 2007.
- Milad Nasr, Jamie Hayes, Thomas Steinke, Borja Balle, Florian Tramèr, Matthew Jagielski, Nicholas Carlini, and Andreas Terzis. Tight auditing of differentially private machine learning. In *USENIX Security Symposium*, 2023.
- Alexandre Sablayrolles, Matthijs Douze, Cordelia Schmid, Yann Ollivier, and Hervé Jégou. White-box vs black-box: Bayes optimal strategies for membership inference. In *International Conference on Machine Learning (ICML)*, pages 5558–5567. PMLR, 2019.
- Ahmed Salem, Yang Zhang, Mathieu Humbert, Pascal Berrang, Mario Fritz, and Michael Backes. ML-Leaks: Model and data independent membership inference attacks and defenses on machine learning models. In *Network and Distributed System Security Symposium (NDSS)*, 2019.
- Reza Shokri, Marco Stronati, Congzheng Song, and Vitaly Shmatikov. Membership inference attacks against machine learning models. In *IEEE Symposium on Security and Privacy (SP)*, pages 3–18. IEEE, 2017.
- Liwei Song and Prateek Mittal. Systematic evaluation of privacy risks of machine learning models. In *USENIX Security Symposium*, 2021.
- Thomas Steinke, Milad Nasr, and Matthew Jagielski. Privacy auditing with one (1) training run. *Advances in Neural Information Processing Systems (NeurIPS)*, 2023.
- Lauren Watson, Chuan Guo, Graham Cormode, and Alexandre Sablayrolles. On the importance of difficulty calibration in membership inference attacks. In *International Conference on Learning Representations (ICLR)*, 2022.
- Jiayuan Ye, Aadyaa Maddi, Sasi Kumar Murakonda, Vincent Bindschaedler, and Reza Shokri. Enhanced membership inference attacks against machine learning models. In *ACM Conference on Computer and Communications Security (CCS)*, pages 3093–3106. ACM, 2022.
- Samuel Yeom, Irene Giacomelli, Matt Fredrikson, and Somesh Jha. Privacy risk in machine learning: Analyzing the connection to overfitting. In *IEEE Computer Security Foundations Symposium (CSF)*, pages 268–282. IEEE, 2018.
- Sergey Zagoruyko and Nikos Komodakis. Wide residual networks. *arXiv preprint arXiv:1605.07146*, 2016.
- Sajjad Zarifzadeh, Philippe Liu, and Reza Shokri. Low-cost high-power membership inference attacks. In *International Conference on Machine Learning (ICML)*. PMLR, 2024.

SUPPLEMENTARY MATERIAL

A EXPONENTIAL-FAMILY DERIVATIONS

This appendix states the log-likelihood ratio implied by each distributional family and discusses parameter estimation for the case when they are used directly for MIA. Derivations of the BASE hierarchy are in Appendix B.

A.1 GENERIC FORM

Recall from Section 3 that each distributional family models a scalar statistic z under the two membership classes $m \in \{0, 1\}$, where $m = 1$ denotes IN and $m = 0$ denotes OUT. We assume $z \mid m$ follows an exponential-family distribution

$$p(z \mid m) = h(z) \exp(\eta_m^\top T(z) - A(\eta_m)),$$

with sufficient statistics $T(z)$, natural parameters η_m , base measure $h(z)$, and log-partition function A (4). The log-likelihood ratio for membership is

$$\text{LLR}(z) = (\eta_1 - \eta_0)^\top T(z) - (A(\eta_1) - A(\eta_0)),$$

restating (5). The LLR is affine in $T(z)$: the optimal membership score is a linear combination of the sufficient statistics plus a constant offset. If some components of $T(z)$ are nonlinear in z (e.g., z^2 in the Gaussian), the LLR becomes nonlinear in z unless the corresponding natural parameters are shared across classes. The following subsections specialize this result to four distributional families, identifying the sufficient statistics, natural parameters, and LLR for each.

A.2 EXPONENTIAL SPECIALIZATION

The exponential model operates on the loss statistic $z = \ell$, where $\ell = -\log p$ is the cross-entropy loss and p is the model’s predicted confidence for the ground truth label (see Table 1).

For $\ell \mid m \sim \text{Exp}(\lambda_m)$ with rate $\lambda_m > 0$, the sufficient statistic is $T(\ell) = \ell$, the natural parameter is $\eta_m = -\lambda_m$, and the log-partition function is $A(\eta_m) = -\log \lambda_m$. Substituting into (5):

$$\text{LLR}(\ell) = -(\lambda_1 - \lambda_0)\ell - (-\log \lambda_1 + \log \lambda_0) = \log \frac{\lambda_1}{\lambda_0} - (\lambda_1 - \lambda_0)\ell.$$

The LLR is affine in ℓ with slope $\lambda_0 - \lambda_1$. Since the exponential family has a single sufficient statistic (ℓ itself), the LLR is automatically affine—no parameter constraints are needed to obtain a linear score.

A.3 GAMMA SPECIALIZATION

Like the exponential, the Gamma model operates on the loss statistic $z = \ell$.

For $\ell \mid m \sim \text{Gamma}(\kappa_m, \vartheta_m)$ with shape $\kappa_m > 0$ and scale $\vartheta_m > 0$, the sufficient statistics are $T(\ell) = (\ell, \log \ell)$, the natural parameters are $\eta_m = (-1/\vartheta_m, \kappa_m - 1)$, and the log-partition function is $A(\eta_m) = \log \Gamma(\kappa_m) + \kappa_m \log \vartheta_m$. Substituting into (5) gives the general Gamma LLR:

$$\text{LLR}(\ell) = \left(\frac{1}{\vartheta_0} - \frac{1}{\vartheta_1} \right) \ell + (\kappa_1 - \kappa_0) \log \ell - \log \frac{\Gamma(\kappa_1) \vartheta_1^{\kappa_1}}{\Gamma(\kappa_0) \vartheta_0^{\kappa_0}}.$$

The LLR has two variable terms: one linear in ℓ (driven by the scale difference $1/\vartheta_0 - 1/\vartheta_1$) and one linear in $\log \ell$ (driven by the shape difference $\kappa_1 - \kappa_0$). The constant offset depends on the normalizing constants of both class-conditional distributions.

Under shared scale $\vartheta_0 = \vartheta_1 = \vartheta$, the linear-in- ℓ term vanishes and the LLR simplifies to

$$\text{LLR}(\ell) = (\kappa_1 - \kappa_0) \log \ell - \log \frac{\Gamma(\kappa_1) \vartheta^{\kappa_1}}{\Gamma(\kappa_0) \vartheta^{\kappa_0}},$$

which is affine in $\log \ell$ with slope $\kappa_1 - \kappa_0$. Since $\ell = -\log p$, we have $\log \ell = \log(-\log p)$, so the shared-scale Gamma LLR operates on the log-loss rather than on the loss or confidence directly.

Conversely, under shared shape $\kappa_0 = \kappa_1 = \kappa$, the $\log \ell$ term vanishes and the LLR simplifies to

$$\text{LLR}(\ell) = \left(\frac{1}{\vartheta_0} - \frac{1}{\vartheta_1} \right) \ell - \kappa \log \frac{\vartheta_1}{\vartheta_0},$$

which is affine in ℓ with slope $1/\vartheta_0 - 1/\vartheta_1$. This shared-shape case is structurally identical to the exponential LLR: both are linear in the loss itself.

These two specializations illustrate a general pattern. The shared-scale case (affine in $\log \ell$) retains only the shape difference between classes, while the shared-shape case (affine in ℓ) retains only the scale difference and mirrors the exponential LLR.

A.4 BETA SPECIALIZATION

The Beta model operates on the confidence statistic $z = p$, where p is the model’s predicted probability for the ground truth label. Under cross-entropy loss, $p = e^{-\ell}$, so confidence and loss are related by a monotone transform (see Table 1).

For $p \mid m \sim \text{Beta}(\alpha_m, \beta_m)$ with shape parameters $\alpha_m, \beta_m > 0$, the sufficient statistics are $T(p) = (\log p, \log(1 - p))$, the natural parameters are $\eta_m = (\alpha_m - 1, \beta_m - 1)$, and the log-partition function is $A(\eta_m) = \log B(\alpha_m, \beta_m)$, where B is the Beta function. Substituting into (5):

$$\text{LLR}(p) = (\alpha_1 - \alpha_0) \log p + (\beta_1 - \beta_0) \log(1 - p) - \log \frac{B(\alpha_1, \beta_1)}{B(\alpha_0, \beta_0)}.$$

The LLR is linear in $(\log p, \log(1 - p))$, providing a natural two-parameter extension of the exponential model. With two shape parameters per class (four total), the Beta family can capture asymmetric behaviour near $p = 0$ and $p = 1$ independently.

A.5 GAUSSIAN SPECIALIZATION

The Gaussian model operates on the rescaled logit statistic $z = \varphi$, where $\varphi = \log(p/(1 - p))$ is the log-odds of the ground truth label confidence p . The rescaled logit maps $p \in (0, 1)$ to $\varphi \in (-\infty, +\infty)$, making the Gaussian a natural model for this statistic (see Table 1). This is the distributional model underlying LiRA [Carlini et al., 2022].

For $\varphi \mid m \sim \mathcal{N}(\mu_m, \sigma_m^2)$, the sufficient statistics are $T(\varphi) = (\varphi, \varphi^2)$, the natural parameters are $\eta_m = (\mu_m/\sigma_m^2, -1/(2\sigma_m^2))$, and the log-partition function is $A(\eta_m) = \mu_m^2/(2\sigma_m^2) + \log \sigma_m$. Substituting into (5) and simplifying gives the full Gaussian LLR:

$$\text{LLR}(\varphi) = \frac{(\varphi - \mu_0)^2}{2\sigma_0^2} - \frac{(\varphi - \mu_1)^2}{2\sigma_1^2} + \log \frac{\sigma_0}{\sigma_1}.$$

This is the full Gaussian LLR (7), written out here for reference. The LLR is quadratic in φ whenever $\sigma_0 \neq \sigma_1$, because the φ^2 coefficient $\frac{1}{2\sigma_0^2} - \frac{1}{2\sigma_1^2}$ is nonzero. This nonlinearity allows the Gaussian model to capture differences in the spread of shadow statistics between IN and OUT, not just shifts in location.

Under equal variances $\sigma_0^2 = \sigma_1^2 = \sigma^2$, the quadratic terms cancel and the LLR simplifies to

$$\text{LLR}(\varphi) = \frac{\mu_1 - \mu_0}{\sigma^2} \left(\varphi - \frac{\mu_1 + \mu_0}{2} \right),$$

restating (8). This is linear in φ : the slope is proportional to the mean gap $\mu_1 - \mu_0$ and inversely proportional to the variance, while the intercept is set by the midpoint of the two class means.

A.6 PARAMETER ESTIMATION

When using these distributional families for membership inference, we estimate class-conditional parameters from shadow-model statistics. For a given audit point i , the K shadow models produce statistics $z_{i,1}, \dots, z_{i,K}$, each labeled by membership $m_{i,k} \in \{0, 1\}$, where $m = 1$ denotes *IN* (point i was in the training set of shadow model k) and $m = 0$ denotes *OUT*. Let $\mathcal{K}_{i,m} = \{k : m_{i,k} = m\}$ be the index set for each class. Parameters are estimated separately per class and per audit point.

Exponential. The exponential model has one parameter per class: the rate $\lambda_{i,m}$. The MLE is the reciprocal of the sample mean loss:

$$\hat{\lambda}_{i,m} = \frac{1}{\bar{\ell}_{i,m}}, \quad \text{where} \quad \bar{\ell}_{i,m} = \frac{1}{|\mathcal{K}_{i,m}|} \sum_{k \in \mathcal{K}_{i,m}} \ell_{i,k}.$$

Gamma. The Gamma model has two parameters per class: shape $\kappa_{i,m}$ and scale $\vartheta_{i,m}$. No closed-form MLE exists. The profile log-likelihood yields the implicit equation

$$\log \hat{\kappa}_{i,m} - \psi(\hat{\kappa}_{i,m}) = \log \bar{\ell}_{i,m} - \overline{\log \ell}_{i,m},$$

where ψ is the digamma function and

$$\overline{\log \ell}_{i,m} = \frac{1}{|\mathcal{K}_{i,m}|} \sum_{k \in \mathcal{K}_{i,m}} \log \ell_{i,k}$$

is the sample mean of the log-losses. This equation is solved numerically (e.g. Newton–Raphson), after which the scale estimate follows as $\hat{\vartheta}_{i,m} = \bar{\ell}_{i,m} / \hat{\kappa}_{i,m}$.

For initialization, method-of-moments estimates are convenient:

$$\hat{\kappa}_{i,m}^{\text{MoM}} = \frac{\bar{\ell}_{i,m}^2}{s_{i,m}^2}, \quad \hat{\vartheta}_{i,m}^{\text{MoM}} = \frac{s_{i,m}^2}{\bar{\ell}_{i,m}},$$

where $s_{i,m}^2 = |\mathcal{K}_{i,m}|^{-1} \sum_{k \in \mathcal{K}_{i,m}} (\ell_{i,k} - \bar{\ell}_{i,m})^2$ is the sample variance.

Beta. The Beta model has two parameters per class: $\alpha_{i,m}$ and $\beta_{i,m}$. The MLE requires solving the coupled digamma equations

$$\begin{aligned} \psi(\hat{\alpha}_{i,m}) - \psi(\hat{\alpha}_{i,m} + \hat{\beta}_{i,m}) &= \overline{\log p}_{i,m}, \\ \psi(\hat{\beta}_{i,m}) - \psi(\hat{\alpha}_{i,m} + \hat{\beta}_{i,m}) &= \overline{\log(1-p)}_{i,m}, \end{aligned}$$

where

$$\overline{\log p}_{i,m} = \frac{1}{|\mathcal{K}_{i,m}|} \sum_{k \in \mathcal{K}_{i,m}} \log p_{i,k}, \quad \overline{\log(1-p)}_{i,m} = \frac{1}{|\mathcal{K}_{i,m}|} \sum_{k \in \mathcal{K}_{i,m}} \log(1 - p_{i,k}).$$

These are solved numerically, using probability-weighted moment (PWM) estimators for initialization.

Gaussian. The Gaussian model has two parameters per class: mean $\mu_{i,m}$ and variance $\sigma_{i,m}^2$. The MLEs are the sample mean and variance:

$$\hat{\mu}_{i,m} = \frac{1}{|\mathcal{K}_{i,m}|} \sum_{k \in \mathcal{K}_{i,m}} z_{i,k}, \quad \hat{\sigma}_{i,m}^2 = \frac{1}{|\mathcal{K}_{i,m}|} \sum_{k \in \mathcal{K}_{i,m}} (z_{i,k} - \hat{\mu}_{i,m})^2.$$

The BASE hierarchy (Appendix B) introduces parameter-sharing constraints that reduce the number of free parameters. BASE3 pools the variance across the two classes while estimating means separately. BASE2 additionally constrains the mean gap to be constant across data points. BASE1 collapses to a single pooled centering estimate, discarding all per-class variance information.

Robust estimation. Standard MLE estimates can be sensitive to outlier shadow statistics—for instance, a single anomalously low loss can heavily influence the exponential rate estimate. Several robust alternatives exist:

- *Trimmed means:* discard the most extreme fraction of shadow statistics before computing the sample mean.
- *Winsorized variance:* clamp extreme values to a quantile threshold before computing variance, reducing the influence of heavy tails.
- *Median-based estimators:* replace the sample mean with the median, which has a bounded influence function.
- *Interquartile range (IQR):* use the IQR as a robust spread estimate in place of the standard deviation, avoiding sensitivity to extreme tails.
- *Log-sum-exp averaging:* estimate the pooled center via $\hat{z}_{i,\text{pool}} = -\log(\frac{1}{K} \sum_{k=1}^K e^{-\ell_{i,k}})$ instead of the arithmetic mean. This is equivalent to the softmin and provides a natural robust centering in the confidence domain.

We explored trimmed means, winsorized variance, and median-based alternatives in our experiments, but did not find that they improved MIA performance over standard MLE. The exception is log-sum-exp averaging for BASE1, which provides a modest improvement and is used in the standard BASE implementation [Lassila et al., 2025].

B BASE HIERARCHY: DERIVATIONS AND FORMULAS

We now fix a target point i and write LLR_i for its per-datapoint membership log-likelihood ratio. The K shadow statistics $z_{i,1}, \dots, z_{i,K}$ are split by membership label $m_{i,k} \in \{0, 1\}$. Each BASE variant follows from the exponential-family LLR (Appendix A) under specific parameter-sharing constraints. We present the hierarchy top-down, from the most flexible (BASE4) to the most constrained (BASE1).

Sign convention. Since the IN model has been trained on the target point while the OUT model has not, we generally expect higher confidence for IN: $p_{\text{IN}} > p_{\text{OUT}}$, equivalently $-\ell_{\text{IN}} > -\ell_{\text{OUT}}$ and $\varphi_{\text{IN}} > \varphi_{\text{OUT}}$. Throughout the derivations below we therefore choose the scalar statistic $z \in \{p, -\ell, \varphi\}$ so that the IN–OUT mean difference $\Delta\mu := \mu_{i,1} - \mu_{i,0}$ is positive. This convention ensures that the LLR slope is positive and membership scores increase with the target statistic.

BASE4 (full Gaussian, 4 per-point parameters). Assume $z_{i,k} \mid m \sim \mathcal{N}(\mu_{i,m}, \sigma_{i,m}^2)$ with all four parameters $(\mu_{i,0}, \sigma_{i,0}^2, \mu_{i,1}, \sigma_{i,1}^2)$ free. Substituting maximum-likelihood estimates into the Gaussian LLR (7) gives the BASE4 score (12):

$$\text{BASE4}_i = \frac{(z_{i,0} - \hat{\mu}_{i,0})^2}{2\hat{\sigma}_{i,0}^2} - \frac{(z_{i,0} - \hat{\mu}_{i,1})^2}{2\hat{\sigma}_{i,1}^2} + \log \frac{\hat{\sigma}_{i,0}}{\hat{\sigma}_{i,1}}.$$

BASE3 (equal variance, 3 per-point parameters). Constrain $\sigma_{i,0}^2 = \sigma_{i,1}^2 = \sigma_i^2$. The equal-variance Gaussian LLR (8) is linear in z :

$$\text{LLR}_i(z) = \frac{\mu_{i,1} - \mu_{i,0}}{\sigma_i^2} \left(z_{i,0} - \frac{\mu_{i,1} + \mu_{i,0}}{2} \right).$$

Substituting MLE estimates yields the BASE3 score (11):

$$\text{BASE3}_i = \frac{\hat{\mu}_{i,1} - \hat{\mu}_{i,0}}{\hat{\sigma}_i^2} \left(z_{i,0} - \frac{\hat{\mu}_{i,1} + \hat{\mu}_{i,0}}{2} \right),$$

with the estimators

$$\hat{\mu}_{i,m} = \frac{1}{|\mathcal{K}_{i,m}|} \sum_{k \in \mathcal{K}_{i,m}} z_{i,k}, \quad \hat{\sigma}_i^2 = \frac{1}{|\mathcal{K}_{i,0}| + |\mathcal{K}_{i,1}|} \sum_{m \in \{0,1\}} \sum_{k \in \mathcal{K}_{i,m}} (z_{i,k} - \hat{\mu}_{i,m})^2.$$

BASE2 (constant mean gap, 2 per-point parameters). Additionally constrain $\mu_{i,1} - \mu_{i,0} = \Delta\mu$ for all i . The LLR slope $\Delta\mu/\sigma_i^2$ now varies only through the per-point variance; since $\Delta\mu > 0$ is constant, the ranking across data points is determined by

$$\text{BASE2}_i = \frac{z_{i,0} - \hat{\mu}_{i,\text{pool}}}{\hat{\sigma}_i^2},$$

with pooled estimators that ignore membership labels:

$$\hat{\mu}_{i,\text{pool}} = \frac{1}{K} \sum_{k=1}^K z_{i,k}, \quad \hat{\sigma}_i^2 = \frac{1}{K} \sum_{k=1}^K (z_{i,k} - \hat{\mu}_{i,\text{pool}})^2.$$

BASE1 (mean–variance proportionality, 1 per-point parameter). Finally, suppose the means satisfy $\mu_{i,m} = a_m \sigma_i^2$ with constants a_0, a_1 independent of i . Then $\mu_{i,1} - \mu_{i,0} = (a_1 - a_0) \sigma_i^2$, so the equal-variance LLR slope simplifies to the constant $a_1 - a_0$:

$$\text{LLR}_i(z) = (a_1 - a_0)(z_{i,0} - \bar{\mu}_i),$$

where $\bar{\mu}_i = (\mu_{i,1} + \mu_{i,0})/2$. Since $a_1 - a_0 > 0$ is constant across points, the ranking depends only on $z_{i,0} - \bar{\mu}_i$, yielding the BASE1 score (9):

$$\text{BASE1}_i = z_{i,0} - \hat{z}_{i,\text{pool}},$$

where $\hat{z}_{i,\text{pool}}$ estimates the centering $\bar{\mu}_i$ from all K shadow statistics for point i .

Corollary 1 (LiRA = BASE4). Setting $z = \varphi$ (rescaled logits) in the BASE4 formula above and substituting MLE parameters $(\hat{\mu}_{i,m}, \hat{\sigma}_{i,m}^2)$ into (7) recovers the LiRA score (2).

Proof. Direct substitution of MLE $(\hat{\mu}_{i,m}, \hat{\sigma}_{i,m}^2)$ into (7) gives (12), which equals (2). \square

Corollary 2 (BASE = BASE1). *Setting $z = -\ell$ in the BASE1 score and estimating the centering via the log-sum-exp average gives the BASE score of Lassila et al. [2025]:*

$$\text{BASE}_i = -\ell_{i,0} - \log\left(\frac{1}{K} \sum_{k=1}^K e^{-\ell_{i,k}}\right).$$

Proof. Substitute $z = -\ell$ into the BASE1 score $z_{i,0} - \hat{z}_{i,\text{pool}}$. For the centering estimate, replace the arithmetic loss-domain average with its Jensen-stable confidence-domain counterpart $\hat{z}_{i,\text{pool}} = \log(K^{-1} \sum_k e^{-\ell_{i,k}})$, giving the standard BASE formula. \square

Independent derivation: BASE from the exponential model. Assume $\ell_{i,k} \mid m \sim \text{Exp}(\lambda_{i,m})$ with a constant rate gap $\lambda_{i,1} - \lambda_{i,0} = \Delta\lambda > 0$ across data points. The exponential LLR (6) for point i is

$$\text{LLR}_i(\ell) = \log \frac{\lambda_{i,1}}{\lambda_{i,0}} - (\lambda_{i,1} - \lambda_{i,0}) \ell_{i,0},$$

which is exactly affine in the target loss. Under the constant-gap assumption, the slope $-\Delta\lambda$ is common to all points. Introduce the pooled rate $\lambda_{i,\text{pool}} = (\lambda_{i,1} + \lambda_{i,0})/2$ and rewrite the intercept:

$$\log \frac{\lambda_{i,1}}{\lambda_{i,0}} = \log \frac{\lambda_{i,\text{pool}} + \Delta\lambda/2}{\lambda_{i,\text{pool}} - \Delta\lambda/2} \approx \frac{\Delta\lambda}{\lambda_{i,\text{pool}}},$$

where the approximation holds for $\Delta\lambda/\lambda_{i,\text{pool}} \ll 1$. Substituting yields the approximate LLR

$$\text{LLR}_i(\ell) \approx \Delta\lambda \left(\frac{1}{\lambda_{i,\text{pool}}} - \ell_{i,0} \right).$$

Since $\Delta\lambda > 0$ is constant, the ranking depends only on $\lambda_{i,\text{pool}}^{-1} - \ell_{i,0}$. The pooled rate inverse $\lambda_{i,\text{pool}}^{-1}$ is the expected loss under the pooled model, estimated by the sample mean $\hat{\ell}_{i,\text{pool}} = K^{-1} \sum_k \ell_{i,k}$ or the Jensen-stable log-sum-exp average. The latter choice yields

$$\text{BASE}_i = -\ell_{i,0} - \log\left(\frac{1}{K} \sum_{k=1}^K e^{-\ell_{i,k}}\right)$$

Independent derivation: BASE from the Gamma model. Consider a Gamma model on the *confidence*: $p_{i,k} \mid m \sim \text{Gamma}(\kappa_{i,m}, \vartheta_i)$ with a per-point scale $\vartheta_i > 0$ shared across membership classes. Assume a constant shape gap $\kappa_{i,1} - \kappa_{i,0} = \Delta\kappa > 0$ across data points. Under the shared-scale Gamma model, the density is $f(p \mid \kappa, \vartheta) = [\Gamma(\kappa) \vartheta^\kappa]^{-1} p^{\kappa-1} e^{-p/\vartheta}$, and the LLR for the target confidence $p_{i,0}$ is

$$\text{LLR}_i(p_{i,0}) = (\kappa_{i,1} - \kappa_{i,0}) \log p_{i,0} - (\kappa_{i,1} - \kappa_{i,0}) \log \vartheta_i - \log \frac{\Gamma(\kappa_{i,1})}{\Gamma(\kappa_{i,0})}.$$

Since $\log p_{i,0} = -\ell_{i,0}$, this becomes

$$\text{LLR}_i = -\Delta\kappa \ell_{i,0} - \Delta\kappa \log \vartheta_i - \log \frac{\Gamma(\kappa_{i,1})}{\Gamma(\kappa_{i,0})}.$$

The slope $-\Delta\kappa$ is constant across points, so the ranking depends on $-\ell_{i,0} - \log \vartheta_i$ (the log-Gamma ratio varies slowly for moderate shape variation). The shared scale ϑ_i is estimated by the pooled mean of the shadow confidences:

$$\hat{\vartheta}_i = \frac{1}{K} \sum_{k=1}^K p_{i,k} = \frac{1}{K} \sum_{k=1}^K e^{-\ell_{i,k}}.$$

Substituting $\hat{\vartheta}_i$ and dropping the constant $\Delta\kappa$ gives

$$\text{LLR}_i \propto -\ell_{i,0} - \log\left(\frac{1}{K} \sum_{k=1}^K e^{-\ell_{i,k}}\right),$$

recovering the BASE score with log-sum-exp centering.

Remark (unifying principle). All three BASE derivations share a common structure: the distributional LLR is affine in a scalar statistic with a slope that is constant across data points, so membership inference reduces to pooled centering. More generally, in any one-parameter exponential family with sufficient statistic $T(z)$, the LLR is

$$\text{LLR}_i(z) = (\eta_{i,1} - \eta_{i,0})T(z_{i,0}) - (A(\eta_{i,1}) - A(\eta_{i,0})).$$

If the parameter gap $\eta_{i,1} - \eta_{i,0} = \Delta\eta$ is constant across data points, the slope is constant and the score ranking reduces to $T(z_{i,0})$ minus a per-point centering term—exactly the BASE1 structure. The three derivations above are instances with $T(\ell) = \ell$ (exponential), $T(z) = z$ (Gaussian with mean–variance proportionality), and $T(p) = \log p = -\ell$ (shared-scale Gamma on confidence). In each case, centering in the confidence domain via $K^{-1} \sum e^{-\ell_{i,k}}$ yields the log-sum-exp average of the standard BASE implementation [Lassila et al., 2025].

C BAVARIA DETAILS

C.1 NIG POSTERIOR UPDATES

The NIG prior $(\mu, \sigma^2) \sim \text{NIG}(\mu_{\emptyset,m}, \kappa_{\emptyset}, \alpha_{\emptyset}, \beta_{\emptyset,m})$ has density

$$p(\mu, \sigma^2) = \frac{\sqrt{\kappa_{\emptyset}}}{\sigma\sqrt{2\pi}} \frac{\beta_{\emptyset,m}^{\alpha_{\emptyset}}}{\Gamma(\alpha_{\emptyset})} \left(\frac{1}{\sigma^2}\right)^{\alpha_{\emptyset}+1} \exp\left(-\frac{2\beta_{\emptyset,m} + \kappa_{\emptyset}(\mu - \mu_{\emptyset,m})^2}{2\sigma^2}\right).$$

For a fixed data point i and class m , after observing $n_m = |\mathcal{K}_{i,m}|$ shadow statistics with sample mean \bar{z}_m and sum of squared deviations $S_m = \sum_{k \in \mathcal{K}_{i,m}} (z_{i,k} - \bar{z}_m)^2$, the posterior hyperparameters $(\mu'_{i,m}, \kappa'_{i,m}, \alpha'_{i,m}, \beta'_{i,m})$ are given by (14).

C.2 EMPIRICAL BAYES HYPERPARAMETERS

The prior is estimated separately for each class $m \in \{0, 1\}$ via empirical Bayes, pooling shadow statistics across all points:

- $\mu_{\emptyset,m}$: global mean of the statistic across all class- m shadow observations.
- κ_{\emptyset} : controls the strength of the mean prior; set to 1 (weakly informative).
- α_{\emptyset} : controls the strength of the variance prior; set to 2 (weakly informative, ensuring $\mathbb{E}[\sigma^2]$ is finite).
- $\beta_{\emptyset,m}$: set to $\sigma_{m,\text{global}}^2 \cdot (\alpha_{\emptyset} - 1)$, so that $\mathbb{E}[\sigma^2] = \beta_{\emptyset,m}/(\alpha_{\emptyset} - 1)$ matches the observed class- m global variance. With $\alpha_{\emptyset} = 2$, this gives $\beta_{\emptyset,m} = \sigma_{m,\text{global}}^2$.

The strength parameters κ_{\emptyset} and α_{\emptyset} are shared across classes. These defaults are used throughout all experiments. No per-dataset tuning is performed.

C.3 CONVERGENCE TO LIRA

As the number of shadow observations $n_m = |\mathcal{K}_{i,m}|$ grows, the NIG posterior concentrates around the maximum likelihood estimates. Specifically, from the update equations (14)

- The posterior mean converges to the sample mean: $\mu'_{i,m} = \frac{\kappa_{\emptyset}\mu_{\emptyset,m} + n_m\bar{z}_m}{\kappa_{\emptyset} + n_m} \rightarrow \bar{z}_m$ as $n_m \rightarrow \infty$, since the prior contribution $\kappa_{\emptyset}\mu_{\emptyset,m}$ becomes negligible.
- The posterior variance converges to the MLE variance: $\beta'_{i,m}/\alpha'_{i,m} \rightarrow S_m/n_m = \hat{\sigma}_m^2$, so the Bayesian shrinkage vanishes.
- The degrees of freedom $\nu_{i,m} = 2\alpha'_{i,m} = 2\alpha_{\emptyset} + n_m \rightarrow \infty$, so the Student- t predictive (15) converges to a Gaussian.

Consequently, BaVarIA- n reduces to LiRA (same Gaussian LLR with MLE parameters), and BaVarIA- t also reduces to LiRA since the Student- t converges to the Gaussian. The prior becomes non-informative, and all three methods produce identical scores.

Table 3: TPR@0.01 for the BASE hierarchy at $K = 8$ (32 replicates). Bold: best method per dataset.

Dataset	BASE1	BASE2	BASE3	BASE4	LiRA	RMIA
C10-WRN	0.081	0.039	0.070	0.019	0.107	0.081
C100-WRN	0.191	0.070	0.122	0.036	0.157	0.191
CN10-WRN	0.114	0.011	0.112	0.042	0.161	0.114
Loc-4	0.160	0.053	0.230	0.097	0.267	0.160
Pur-4	0.037	0.014	0.029	0.013	0.039	0.037
Tex-4	0.237	0.016	0.211	0.083	0.237	0.237

D FULL EXPERIMENTAL RESULTS

All experiments use Design B resampling with 32 replicates across 12 datasets and 7 shadow-model budgets ($K \in \{4, 8, 16, 32, 64, 128, 254\}$). Figures 5–8 show the online BASE hierarchy scaling curves; Figures 9–12 include both online (solid) and offline (dashed) BaVarIA curves. Tables below show one representative architecture per data source (WideResNet for image, MLP-4 for tabular); the second variant follows the same trends.

D.1 VERIFICATION OF EQUIVALENCES

BASE1 = RMIA. BASE1 on loss with log-sum-exp averaging reproduces RMIA at $\gamma = 1$ exactly ($\max |\Delta\text{AUC}| = 0$ across all K and datasets), confirming the equivalence of Lassila et al. [2025].

BASE4 = LiRA. BASE4 on rescaled logits with MLE parameters (denominator n , i.e., the biased variance estimator) reproduces LiRA exactly at $K \geq 64$ ($\max |\Delta\text{AUC}| < 10^{-6}$). At $K < 64$, LiRA’s hard switch substitutes a global variance for the per-point MLE, breaking the equivalence ($\max |\Delta\text{AUC}| = 0.039$ at $K = 8$).

D.2 BASE HIERARCHY AT MULTIPLE SHADOW BUDGETS

Tables 3 and 4 report TPR@0.01 for the full BASE hierarchy at $K = 8$ and $K = 64$. At $K = 8$, LiRA dominates most datasets thanks to numerical safeguards, while raw MLE (BASE4) collapses to near-random (TPR@0.01 = 0.019 on C10-WRN)—confirming that per-class variance estimation from ~ 4 observations is unreliable. BASE1 (= RMIA) is competitive because pooled centering avoids the IN/OUT split. At $K = 64$, BASE3 (pooled variance) outperforms LiRA (e.g., 0.141 vs. 0.078 on C10-WRN): with ~ 32 observations per class, means are stable but per-class variances remain noisy, so pooling provides a more reliable denominator. At $K = 254$ (Table 2), the advantage reverses as LiRA’s per-class variances converge.

LiRA’s hard-switch discontinuity. Conventional LiRA implementations switch from a single global variance to per-point variance estimation at $K = 64$ (i.e., when at least 32 observations are available per class). This binary switch produces a visible kink in LiRA’s scaling curve: the step gain from $K = 32$ to $K = 64$ is anomalously large compared to the otherwise monotonically decreasing marginal returns at adjacent K values (Figures 7–8). The effect is most pronounced for TPR@0.01, where the variance term in the Gaussian LLR has the greatest influence on tail behavior. Conversely, BaVarIA- n ’s advantage over LiRA peaks at $K = 32$ —where LiRA is still constrained to global variance—and drops sharply at $K = 64$ once LiRA switches to per-point estimation. BaVarIA avoids this discontinuity entirely: the NIG posterior smoothly shifts weight from the global prior to per-point data as K grows, producing a monotonically improving scaling curve with no implementation-dependent threshold (Figure 2).

D.3 DISTRIBUTIONAL DIAGNOSTICS

Figure 4 shows QQ plots of per-datapoint standardized shadow log-odds against the $\mathcal{N}(0, 1)$ reference, and Table 5 reports Anderson-Darling (AD) rejection rates at the 5% level for all twelve testbeds. Rejection rates range from near-nominal ($\sim 6\%$ on CIFAR-10 WRN) to over 80% (Location MLP-3 IN class), with the IN class typically showing stronger departures than OUT—consistent with heavier tails visible in the QQ plots for CIFAR-100 ResNet (74% IN rejection).

Despite these departures, the Gaussian-family methods dominate across all datasets (Section 5). The LLR score is evaluated

Table 4: TPR@0.01 for the BASE hierarchy at $K = 64$. BASE3 (pooled variance) slightly outperforms LiRA at this budget.

Dataset	BASE1	BASE2	BASE3	BASE4	LiRA	RMIA
C10-WRN	0.089	0.055	0.141	0.078	0.078	0.089
C100-WRN	0.202	0.087	0.200	0.163	0.163	0.202
CN10-WRN	0.133	0.009	0.187	0.182	0.182	0.133
Loc-4	0.218	0.064	0.420	0.410	0.410	0.218
Pur-4	0.049	0.013	0.064	0.055	0.055	0.049
Tex-4	0.277	0.013	0.357	0.351	0.351	0.277

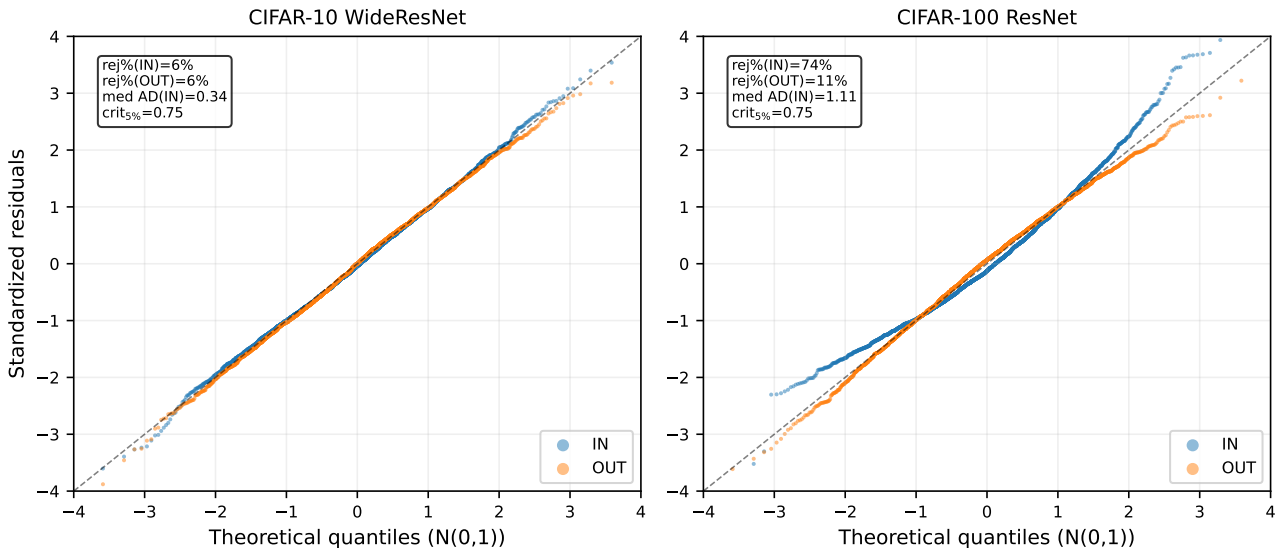


Figure 4: Per-datapoint QQ diagnostic: standardized residuals of shadow log-odds (per data point, per class) pooled across datapoints and plotted against $\mathcal{N}(0, 1)$ quantiles. Annotations show per-datapoint Anderson-Darling (AD) rejection rates. CIFAR-10 WRN is well-approximated by a Gaussian ($\sim 6\%$ AD rejection); CIFAR-100 ResNet shows heavier tails in the IN class (74% AD rejection).

at the target model’s output, which typically lies in the bulk of the distribution where the Gaussian approximation remains accurate; tail departures affect the density estimate but not the ranking of most data points.

E DISTRIBUTION FAMILY COMPARISON

Table 6 compares the four distributional families from the exponential-family framework at $K = 64$. The Gaussian model (on rescaled logits) matches LiRA exactly and dominates all alternatives on every dataset. The Exponential model (on loss) performs poorly, achieving near-random TPR on several datasets (C10-WRN: 0.011, Pur-4: 0.007). This occurs because the exponential’s single rate parameter cannot capture the *variance* differences between IN and OUT that drive discrimination—the LLR is constrained to be linear in the loss.

The Gamma model improves over the Exponential by adding a shape parameter but remains substantially below the Gaussian. The Beta model, operating on confidences with a two-parameter LLR, performs better than Gamma on most datasets but still trails the Gaussian. These results confirm that the choice of sufficient statistic (log-odds vs. loss vs. confidence) matters more than the parametric flexibility of the distributional family.

F BAVARIA PER-DATASET RESULTS

Tables 7 and 8 report per-dataset results for the BaVarIA variants at the shadow budgets where the Bayesian advantage is largest. Figures 9–12 show the full scaling curves across all datasets (solid = online, dashed = offline). We discuss the online

Table 5: Per-datapoint Anderson-Darling normality test on shadow log-odds ($K = 254$, $n = 1,000$ datapoints per class). Rejection rate at the 5% significance level (critical value 0.748). Gaussianity holds well for WideResNet on CIFAR-10/100 but is strongly violated for Location and CINIC-10 WideResNet.

Dataset	IN class		OUT class	
	med AD	rej%	med AD	rej%
C10-RN	0.475	22.4	0.438	19.4
C10-WRN	0.342	5.9	0.355	6.5
C100-RN	1.106	74.3	0.388	11.1
C100-WRN	0.357	6.8	0.369	8.2
CN10-RN	0.607	37.6	0.420	18.2
CN10-WRN	0.934	57.3	1.463	67.2
Loc-3	1.966	85.0	0.402	12.9
Loc-4	1.055	70.5	0.618	41.1
Pur-3	0.403	15.1	0.456	20.4
Pur-4	0.400	15.9	0.437	18.6
Tex-3	0.406	17.2	0.396	14.4
Tex-4	0.437	17.3	0.482	26.7

Table 6: TPR@0.01 by distributional family at $K = 64$. GAUSS on rescaled logits matches LiRA.

Dataset	EXP	GAUSS	GAMMA	BETA	LiRA	RMIA
C10-WRN	0.011	0.078	0.028	0.011	0.078	0.089
C100-WRN	0.010	0.163	0.045	0.064	0.163	0.202
CN10-WRN	0.171	0.182	0.047	0.153	0.182	0.133
Loc-4	0.039	0.410	0.071	0.125	0.410	0.218
Pur-4	0.007	0.055	0.009	0.013	0.055	0.049
Tex-4	0.052	0.351	0.077	0.145	0.351	0.277

Table 7: AUC at $K = 8$ (32 replicates). BaVarIA- t achieves the best AUC on most datasets at this small shadow budget.

Dataset	BaVarIA- n	BaVarIA- t	LiRA	RMIA
C10-WRN	0.673	0.702	0.664	0.679
C100-WRN	0.854	0.824	0.778	0.828
CN10-WRN	0.673	0.730	0.726	0.708
Loc-4	0.860	0.927	0.915	0.831
Pur-4	0.615	0.624	0.619	0.637
Tex-4	0.805	0.876	0.869	0.855

Table 8: TPR@0.001 at $K = 64$. Bayesian variance shrinkage provides dramatic improvements in the extreme tails.

Dataset	BaVarIA- n	BaVarIA- t	LiRA	RMIA
C10-WRN	0.059	0.048	0.014	0.034
C100-WRN	0.098	0.067	0.039	0.051
CN10-WRN	0.090	0.105	0.085	0.069
Loc-4	0.119	0.261	0.273	0.111
Pur-4	0.011	0.014	0.009	0.011
Tex-4	0.111	0.194	0.181	0.142

results in this section and refer to Appendix I for an analysis of the offline results.

At $K = 8$ (Table 7), BaVarIA- t achieves the best AUC on 4 of 6 datasets. The gains are largest on datasets with strong membership signals: Location (+0.012 vs. LiRA) and CIFAR-10 WRN (+0.038). BaVarIA- n also improves over LiRA on some datasets but less consistently, as its Gaussian LLR cannot exploit the heavier-tailed predictive distribution that helps AUC.

At $K = 64$ on TPR@0.001 (Table 8), the Bayesian advantage is even more dramatic. BaVarIA- n achieves TPR@0.001 = 0.059 on C10-WRN vs. 0.014 for LiRA—a $4.2\times$ improvement—confirming that Bayesian variance shrinkage provides the most benefit in the extreme tails at moderate K , where per-class variance estimates are still noisy enough to produce unreliable LLR scores. On Location, LiRA retains a slight edge (0.273 vs. 0.261 for BaVarIA- t), indicating that the Bayesian prior is already non-informative for datasets where the per-class signal is very strong.

G CROSS-VALIDATION ON INDEPENDENT DATA

To verify that our findings generalize beyond a single training pipeline, we cross-validated all methods on an independent shadow-model collection trained without data augmentation or dropout. This collection provides 224–1,480 shadow models per dataset (vs. 254 in our primary benchmark).

Absolute vulnerability. Models trained without augmentation are substantially more vulnerable to MIA on image datasets: CIFAR-10 ResNet AUC increases from 0.613 to 0.874, CIFAR-100 ResNet from 0.978 to 0.993. This is consistent with the findings of Sablayrolles et al. [2019], who first documented this effect at scale on ImageNet (attack accuracy dropping from 90% to 68% with standard augmentation). On tabular datasets, the difference is smaller since these tasks already lack augmentation.

Method ranking preservation. Despite the large shift in absolute vulnerability, the relative method ranking is fully preserved across both data sources: BaVarIA- $n \geq$ BaVarIA- $t \geq$ LiRA $>$ BASE3 $>$ RMIA $>$ BASE2. At $K = 64$, BaVarIA- n beats LiRA on TPR@0.01 in 10 of 12 datasets. The exceptions are the two CIFAR-100 datasets, where LiRA retains a marginal edge ($|\Delta\text{TPR}| < 0.003$).

Convergence at large K . On the independent data, the convergence of BaVarIA to LiRA is even more apparent because the collection provides up to 1,480 shadow models. At $K = 254$, BaVarIA- n and LiRA produce identical AUC to three decimal places on 6 of 10 available datasets, confirming the theoretical convergence result of Appendix C.

These findings confirm that the BaVarIA advantage at small K , the BASE hierarchy ordering, and the convergence at large

K are robust to differences in training recipes and model regularization.

H ELSA: DISCRIMINATIVE SCORING

For any exponential-family model, the log-likelihood ratio is a linear function of the sufficient statistics (Section 3):

$$\text{LLR}(z) = w^\top \phi(z), \quad (17)$$

where ϕ is a feature map determined by the distributional family. Rather than estimating w generatively (via MLE of the distributional parameters), we can estimate it discriminatively via logistic regression on shadow-model data.

Feature map. We define a universal feature map that subsumes the sufficient statistics of all distributional families considered in this paper:

$$\phi(p) = [1, \log(-\log p), \log p, \log(1-p), \varphi^2, p, p^2]^\top, \quad (18)$$

where $\varphi = \log(p/(1-p))$ is the rescaled logit. Different distributional families correspond to different active subsets of ϕ : the Gaussian model on log-odds uses $\{1, \varphi, \varphi^2\}$, the Beta model uses $\{1, \log p, \log(1-p)\}$, and the Gamma model uses $\{1, \log(-\log p), \log p\}$.

Training. For each data point i , we fit weights w_i by minimizing the ridge-penalized logistic loss over shadow-model observations:

$$\hat{w}_i = \arg \min_w \left[-\sum_{k=1}^K \left(m_{i,k} \log \sigma(w^\top \phi_k) + (1 - m_{i,k}) \log(1 - \sigma(w^\top \phi_k)) \right) + \lambda \|w_{-0}\|^2 \right], \quad (19)$$

where $\phi_k = \phi(p_{i,k})$, σ is the sigmoid function, and λ is the ridge penalty applied to all weights except the intercept w_0 . The intercept is excluded from penalization following standard practice in regularized logistic regression: including it would shrink all predictions toward the 0.5 base rate, preventing the model from learning even the marginal membership probability.

Distribution-specific ELSA variants are obtained by feature masking: setting $w_j = 0$ for features outside the active set forces the model to use only the sufficient statistics of the chosen family. For example, ELSA2 ϕ optimizes only $\{w_0, w_\varphi\}$, recovering a discriminatively trained analogue of the equal-variance Gaussian LLR (8), while ELSA3 ϕ adds w_{φ^2} to capture the full Gaussian structure (7).

Results. Tables 9 and 10 report AUC and TPR@0.001 at $K = 64$ for the ELSA variants. The feature maps correspond to different distributional initializations: ELSA1 uses a single feature (intercept only, equivalent to the exponential model); ELSA2 ϕ uses the rescaled logit φ (two features, inspired by the Gaussian model); ELSA3 β and ELSA3 γ use three features from the Beta and Gamma sufficient statistics; ELSA3 ϕ adds the quadratic term φ^2 ; and ELSA-full uses all seven features.

AUC. On AUC (Table 9), ELSA2 ϕ and ELSA3 β consistently outperform LiRA, with mean improvements of +0.065 and +0.062 respectively. The gains are largest on datasets where the Gaussian LLR is suboptimal: CIFAR-10 (+0.098), Location (+0.059). Interestingly, the simplest two-feature model (ELSA2 ϕ) matches or beats the richer models, suggesting that discriminative training primarily learns a better slope for the Gaussian LLR rather than exploiting non-Gaussian structure.

TPR at low FPR. On TPR@0.001 (Table 10), results are more mixed. ELSA2 ϕ beats LiRA on 4 of 6 datasets, with large gains on CINIC-10 (0.092 vs. 0.041) and Purchase (0.018 vs. 0.004). However, on Location, LiRA retains its advantage (0.214 vs. 0.174). Richer models degrade severely on some datasets: ELSA3 ϕ achieves TPR@0.001 = 0.001 on CIFAR-10, and ELSA-full drops to 0.005. This indicates that ridge regularization shrinks extreme scores toward zero when the feature space is too large relative to K , making feature selection critical.

Practical assessment. ELSA’s discriminative approach provides a useful diagnostic for whether the parametric LLR form is well-specified. However, it requires per-point logistic regression (additional computation) and is sensitive to feature selection—the gap between ELSA2 ϕ (TPR = 0.058) and ELSA3 ϕ (TPR = 0.001) on CIFAR-10 highlights this fragility. For practitioners seeking a simple, robust improvement over LiRA, BaVarIA offers a more reliable path.

Table 9: ELSA: AUC at $K = 64$. Ridge-regularized two-feature models consistently improve over LiRA.

Method	C10	C100	CN10	Loc	Pur	Tex
LiRA	.613	.698	.651	.882	.638	.833
RMIA	.668	.831	.658	.839	.641	.862
ELSA1	.709	.847	.687	.834	.650	.861
ELSA2 ϕ	.711	.799	.707	.941	.650	.895
ELSA3 β	.713	.782	.710	.942	.648	.893
ELSA3 γ	.712	.793	.709	.941	.649	.894
ELSA3 ϕ	.695	.790	.711	.940	.643	.894
ELSA-full	.694	.776	.711	.939	.643	.892

Table 10: ELSA: TPR@0.001 at $K = 64$. Feature selection strongly affects tail performance; richer models can collapse.

Method	C10	C100	CN10	Loc	Pur	Tex
LiRA	0.049	0.070	0.041	0.214	0.004	0.109
RMIA	0.031	0.060	0.047	0.111	0.010	0.154
ELSA1	0.026	0.066	0.035	0.062	0.008	0.103
ELSA2 ϕ	0.058	0.101	0.092	0.174	0.018	0.196
ELSA3 β	0.053	0.067	0.087	0.143	0.015	0.166
ELSA3 γ	0.060	0.092	0.092	0.156	0.017	0.186
ELSA3 ϕ	0.001	0.004	0.063	0.184	0.012	0.122
ELSA-full	0.005	0.003	0.050	0.126	0.010	0.093

I OFFLINE SETTING ANALYSIS

In the online (audit) setting used throughout this paper, each target point appears in roughly half of the shadow-model training sets, providing per-point IN and OUT observations. In the offline (practical) setting, shadow models are trained on data from the same distribution as the target model but the target point does not appear in any shadow training set [Carlini et al., 2022]. All shadow observations for a given target point are therefore OUT-class samples; no direct IN-class observations are available.

Existing offline approaches. LiRA [Carlini et al., 2022] estimates μ_{out} per-point from all (OUT-only) shadows but must approximate μ_{in} via a global mean-shift heuristic: $\hat{\mu}_{\text{in}} = \hat{\mu}_{\text{out}} + \Delta$, where Δ is a population-level constant estimated from reference data. With forced equal variances $\sigma_{\text{in}}^2 = \sigma_{\text{out}}^2 = \sigma^2$, the Gaussian LLR (7) reduces to

$$\text{LLR}_{\text{offline}}(\varphi) = \frac{\Delta}{\sigma^2} \left(\varphi - \hat{\mu}_{\text{out}} - \frac{\Delta}{2} \right), \quad (20)$$

a linear function of the observation—an instance of the equal-variance Gaussian LLR (8) with the shifted mean. This represents a substantial degradation from the full four-parameter online LiRA, particularly at low FPR where per-point heterogeneity carries the strongest signal.

In practice, Carlini et al. [2022] implement the offline attack via the Gaussian log-CDF: $\text{score}_i = \log \Phi((\varphi_{i,0} - \hat{\mu}_{i,\text{out}})/\hat{\sigma})$, where Φ is the standard normal CDF. When $\hat{\sigma}$ is a single global constant (the offline regime), this is a monotone transformation of the linear score (20) and produces the same ROC curve. When $\hat{\sigma}$ varies per-point, the two formulations can differ in ranking.

RMIA [Zarifzadeh et al., 2024] uses a population-reference mechanism that does not explicitly split shadow observations into IN and OUT classes, making its score formula applicable without modification in the offline setting. However, the offline score distribution shifts because all shadow models are OUT-only: the likelihood ratios computed against reference points are systematically biased when the target point never appeared in training. Empirically, RMIA shows a small but consistent degradation in our experiments ($\Delta_{\text{AUC}} \approx 0.008$; Tables 12–13), confirming that the online/offline distinction is not entirely transparent even for reference-based methods.

Table 11: BASE hierarchy: online vs. offline parameter estimation. In the offline setting, methods that estimate separate IN-class parameters collapse toward pooled estimation.

Method	Online parameters	Offline fallback
BASE1	$\hat{z}_{i,\text{pool}}$ from all shadows	Same; optional α scaling (21)
BASE2	$\hat{\mu}_{i,\text{pool}}, \hat{\sigma}_i^2$ from all	Same; all shadows are OUT
BASE3	$\hat{\mu}_{i,0}, \hat{\mu}_{i,1}; \hat{\sigma}_i^2$ pooled	$\hat{\mu}_{i,1} = \hat{\mu}_{i,0} + \Delta$; \rightarrow eq-var LLR
BASE4	$\hat{\mu}_{i,m}, \hat{\sigma}_{i,m}^2$ per class	$\sigma_{\text{in}}^2 = \sigma_{\text{out}}^2, \mu_{\text{in}}$ via shift; \rightarrow eq-var LLR

BASE [Lassila et al., 2025] introduces a scaling factor $\alpha \in [0, 1]$ on the log-sum-exp term for the offline case:

$$\text{BASE}_i^{\text{off}} = -\ell_{i,0} - \alpha \cdot \log\left(\frac{1}{K} \sum_{k=1}^K e^{-\ell_{i,k}}\right), \quad (21)$$

where the sum runs over OUT-only shadow models and α compensates for the systematically higher losses of models that never trained on the target point. The BASE–RMIA equivalence (Proposition 1a) holds only in the online setting; offline, the two attacks diverge due to their different compensation mechanisms [Lassila et al., 2025].

BASE hierarchy in the offline setting. Table 11 summarizes how each BASE variant adapts to the offline case. The key pattern is that methods requiring IN-class parameters lose access to per-point IN observations and must fall back on population-level estimates.

BASE1 and BASE2 are inherently offline-friendly because they never split shadow observations into IN and OUT classes: the pooled estimates use all available shadows regardless of membership status. BASE3 and BASE4, which require separate IN-class parameters, must estimate the missing μ_{in} via a global mean-shift heuristic and force equal variances. Under these constraints, both reduce to the equal-variance Gaussian LLR (8) with the shifted mean—the same functional form as BASE2 (affine in the observation, normalized by pooled variance), differing only in the Δ -dependent centering point.

BaVarIA in the offline setting. BaVarIA’s conjugate NIG prior provides a principled mechanism for the offline case. With zero IN-class observations for the target point ($n_1 = 0$), the NIG posterior updates (14) reduce to the prior: $\mu'_{i,1} = \mu_{\emptyset,1}$, $\kappa'_{i,1} = \kappa_{\emptyset}$, $\alpha'_{i,1} = \alpha_{\emptyset}$, $\beta'_{i,1} = \beta_{\emptyset,1}$. The IN-class parameters are thus set entirely by the empirical Bayes prior.

Crucially, the prior estimation procedure is unchanged between online and offline settings. Even in the offline case, the adversary controls the shadow model training and therefore knows which *reference points* (the shadow models’ own training data, disjoint from the target’s) were IN or OUT for each shadow model. The class-specific priors ($\mu_{\emptyset,m}, \beta_{\emptyset,m}$) are estimated from these reference-point observations (Appendix C), which include both IN and OUT samples. The offline limitation is purely per-point: for the specific target point being audited, the IN-class posterior collapses to the (well-estimated) IN-class prior, while the OUT-class posterior is fully updated from K shadow observations.

This parallels what LiRA’s hard-switch heuristic achieves (global variance when K is small), but BaVarIA obtains it as a smooth limiting case of the same Bayesian machinery used in the online setting. As per-point IN-class observations become available (online setting with increasing K), the posterior smoothly transitions from population-level to per-point estimates. The offline-to-online transition requires no separate implementation or additional hyperparameters.

Experimental results. Figures 9–12 compare online and offline performance for LiRA, RMIA, and the two BaVarIA variants across all testbeds (solid = online, dashed = offline). Tables 12 and 13 report the mean offline performance and the degradation $\Delta = \text{online} - \text{offline}$. All methods show positive degradation: online consistently outperforms offline, as expected. BaVarIA-n achieves the best offline AUC at $K \geq 64$ and the best offline TPR at FPR=0.01 across all K , while BaVarIA-t leads for AUC at $K=8$. RMIA exhibits the smallest degradation ($\Delta_{\text{AUC}} \approx 0.008$), followed by BaVarIA-n ($\Delta_{\text{AUC}} \approx 0.013\text{--}0.034$); LiRA shows the largest gap ($\Delta_{\text{AUC}} \approx 0.033\text{--}0.045$). Overall, the offline setting remains viable across all approaches, with absolute performance differences between methods being more practically relevant than the online-to-offline gap.

No single method dominates: the best offline method varies across metrics and shadow budgets even at a fixed K .

Table 12: Offline AUC (mean over 12 datasets, 32 replicates). Δ = online – offline. Bold: best offline value per K .

Method	$K = 8$		$K = 64$		$K = 254$	
	Off	Δ	Off	Δ	Off	Δ
LiRA	0.755	+0.033	0.772	+0.042	0.775	+0.045
RMIA	0.763	+0.009	0.769	+0.008	0.770	+0.008
BaVarIA-n	0.773	+0.013	0.785	+0.029	0.786	+0.034
BaVarIA-t	0.778	+0.015	0.784	+0.031	0.784	+0.036

Table 13: Offline TPR at FPR=0.01 (mean over 12 datasets, 32 replicates). Δ = online – offline. Bold: best offline value.

Method	$K = 8$		$K = 64$		$K = 254$	
	Off	Δ	Off	Δ	Off	Δ
LiRA	0.174	+0.034	0.216	+0.050	0.233	+0.051
RMIA	0.144	+0.013	0.180	+0.013	0.185	+0.013
BaVarIA-n	0.200	+0.014	0.246	+0.027	0.254	+0.031
BaVarIA-t	0.196	+0.005	0.242	+0.029	0.249	+0.035

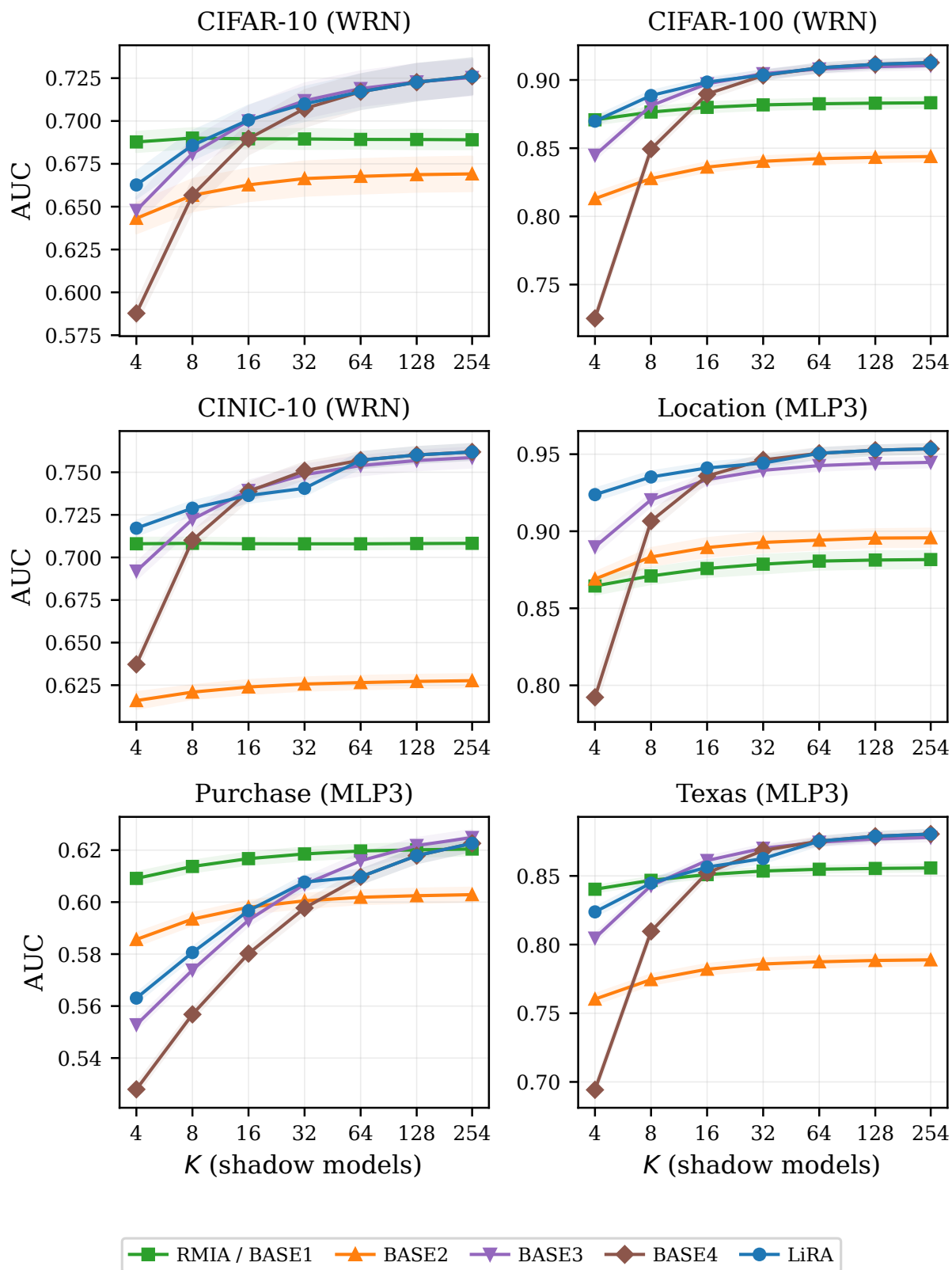


Figure 5: Online AUC vs. K for the BASE hierarchy (WRN/MLP3 testbeds). BASE3 (pooled variance) overtakes LiRA/BASE4 at moderate K ; RMIA/BASE1 lags at all budgets.

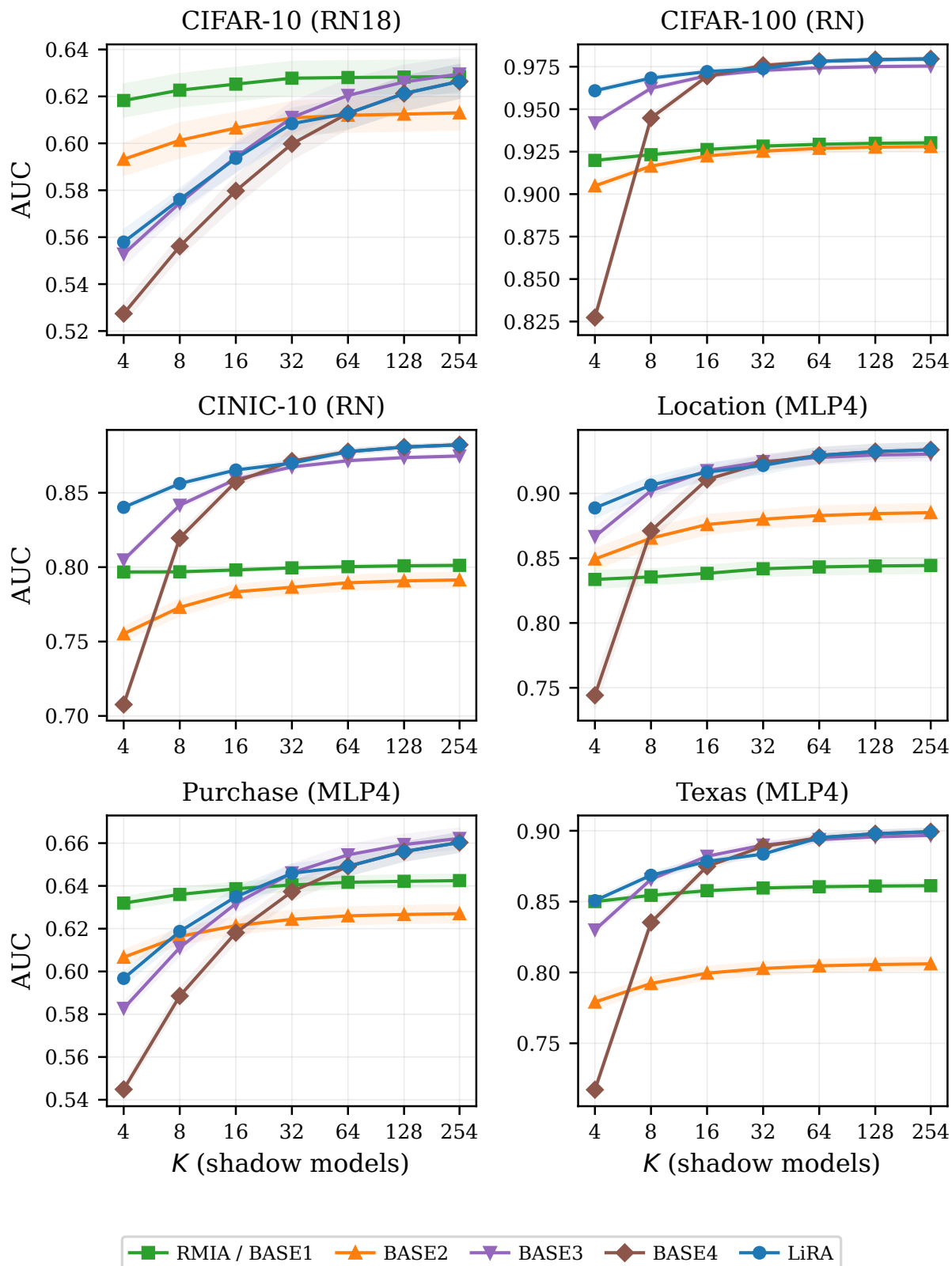


Figure 6: Online AUC vs. K for the BASE hierarchy (RN18/MLP4 testbeds).

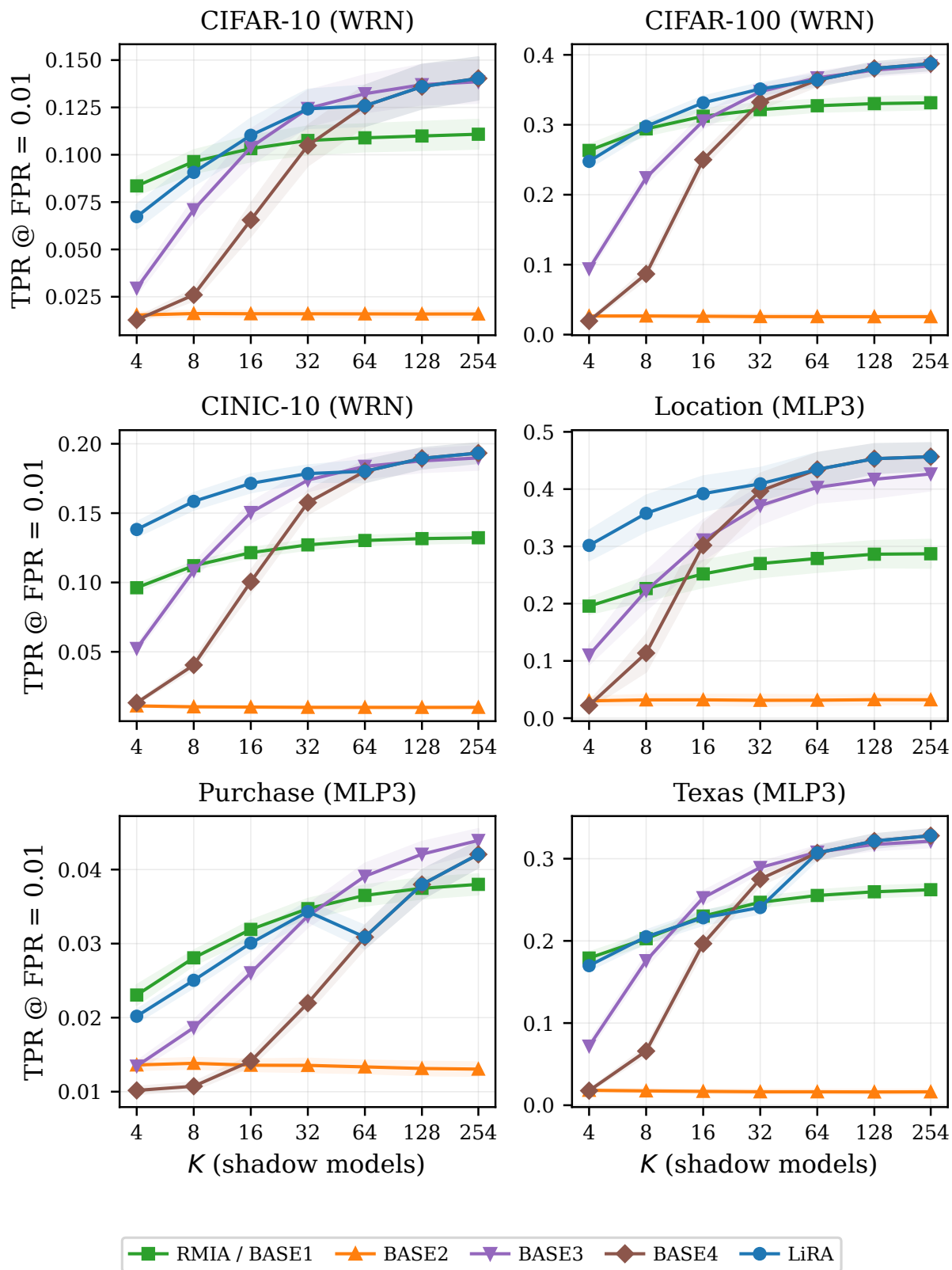


Figure 7: Online TPR at FPR=0.01 vs. K for the BASE hierarchy (WRN/MLP3 testbeds).

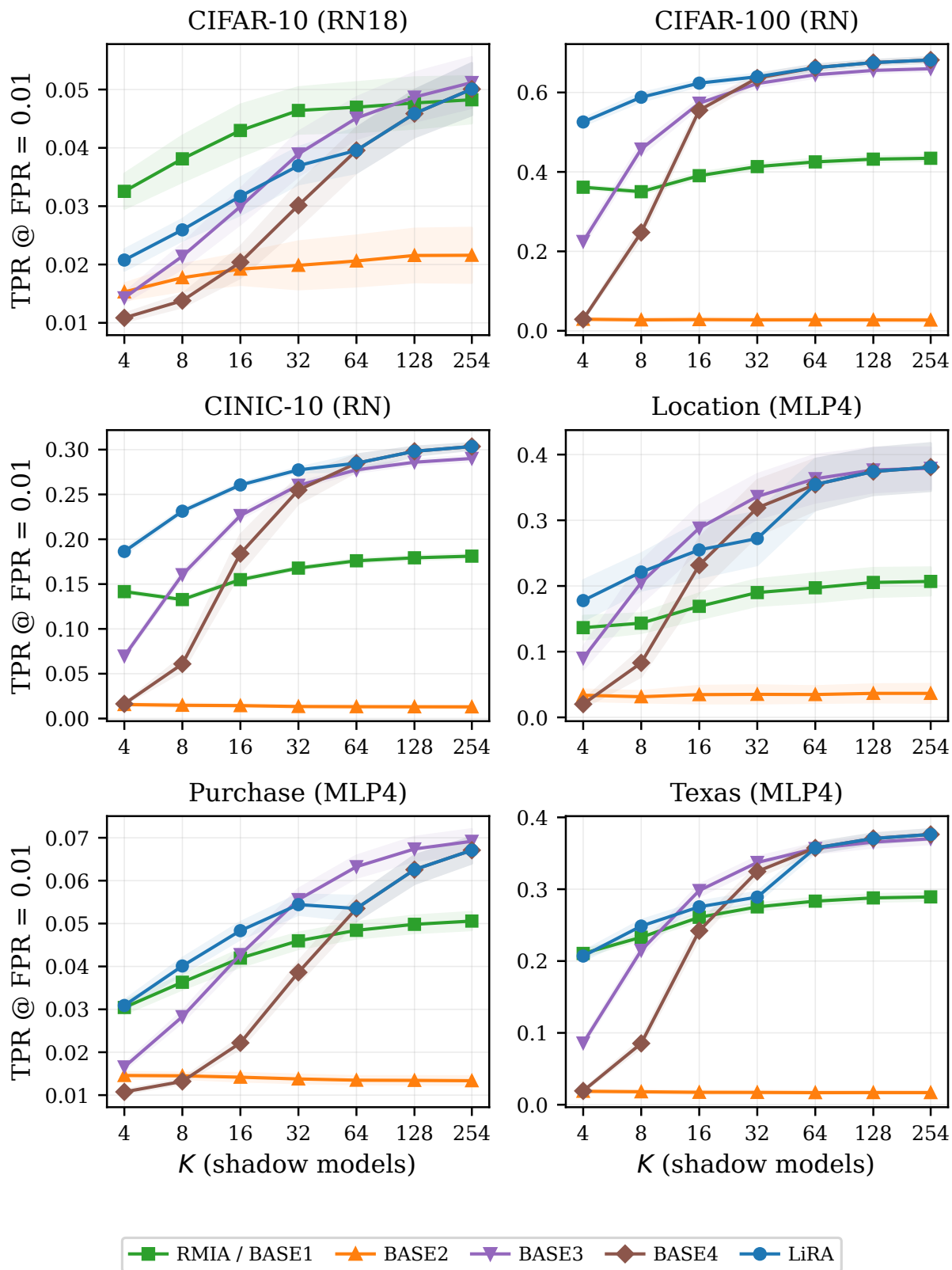


Figure 8: Online TPR at FPR=0.01 vs. K for the BASE hierarchy (RN18/MLP4 testbeds).

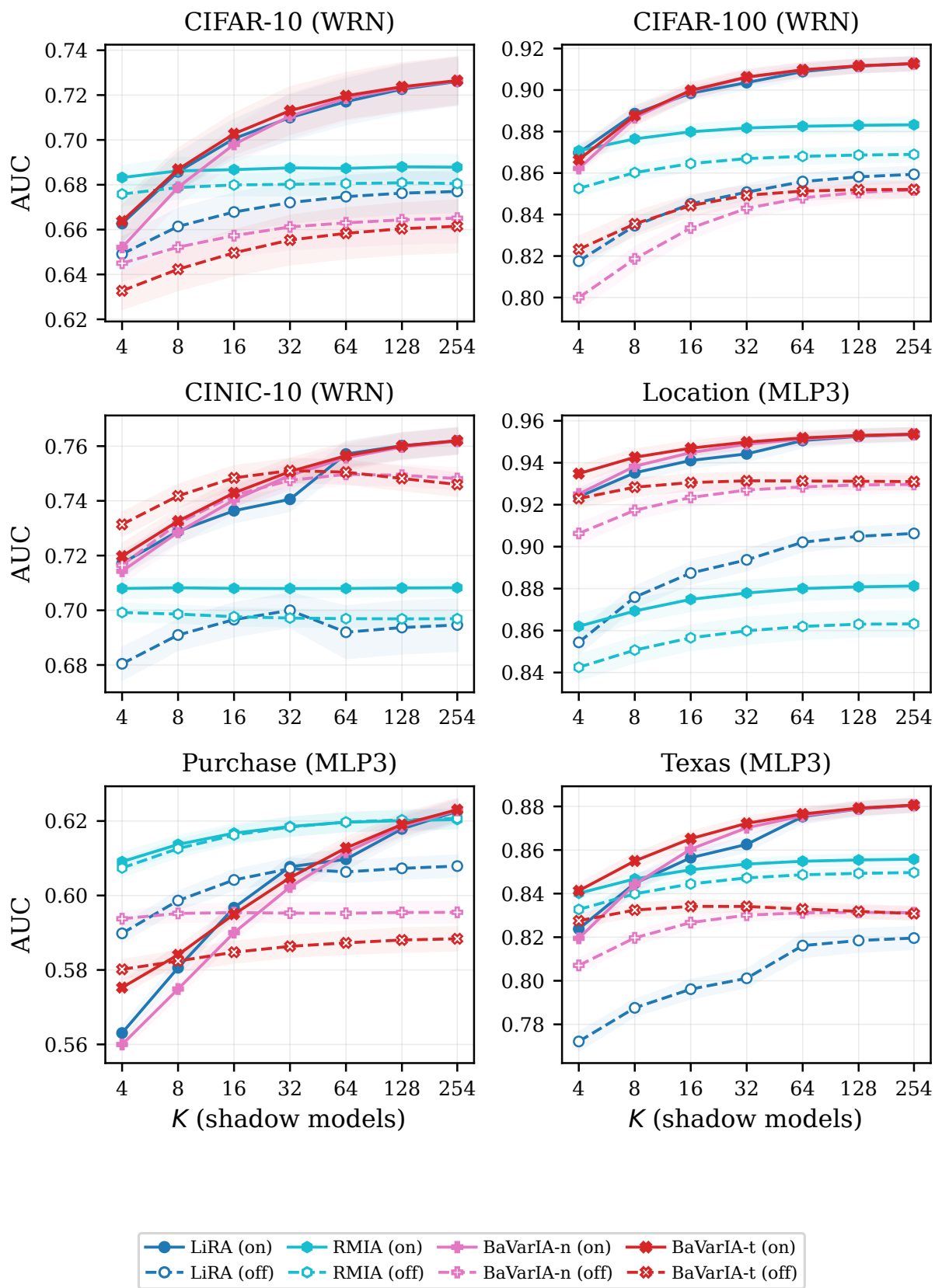


Figure 9: Online vs. offline AUC as a function of K (WRN/MLP3 testbeds). Solid = online, dashed = offline.

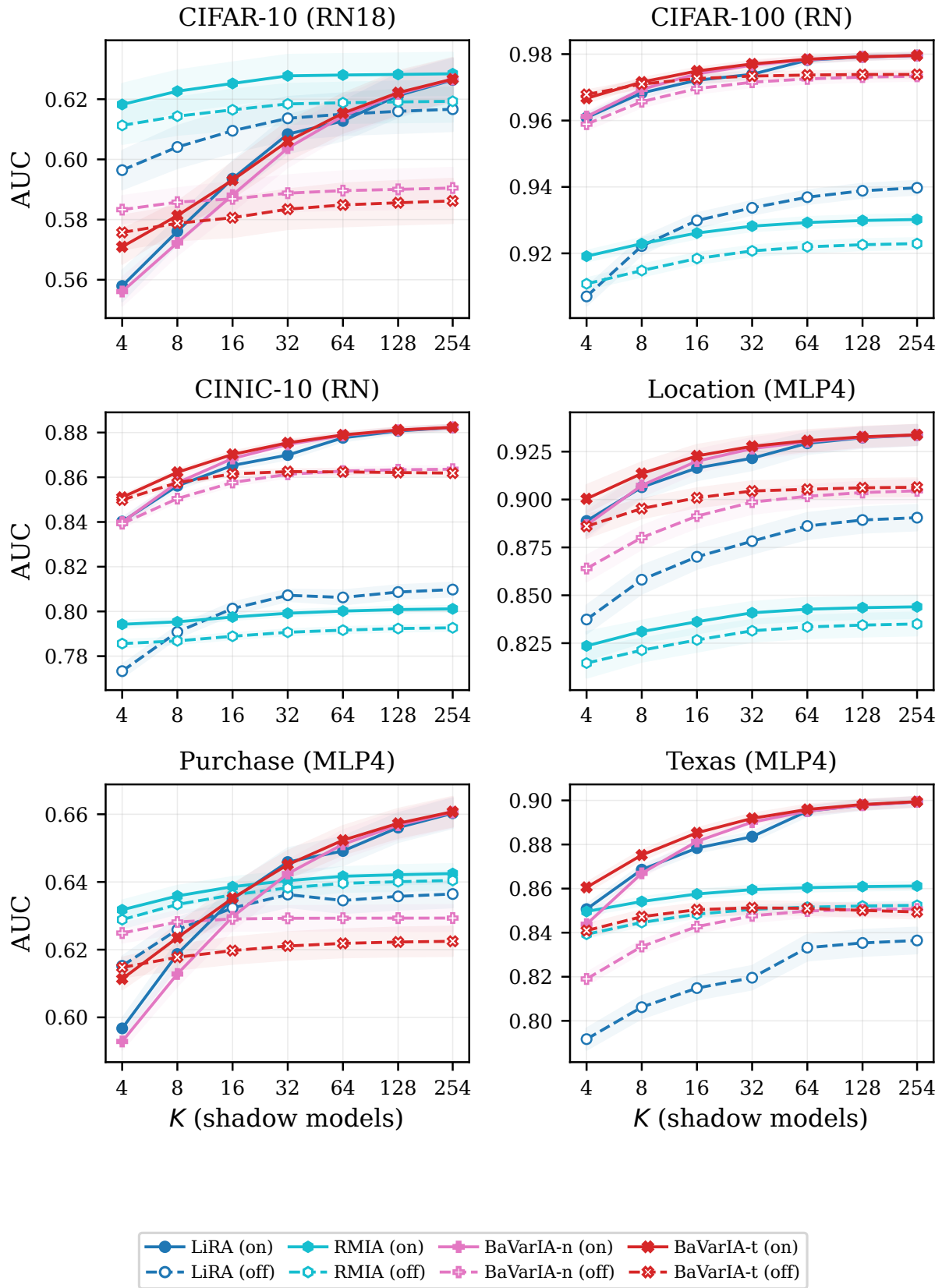


Figure 10: Online vs. offline AUC as a function of K (RN18/MLP4 testbeds).

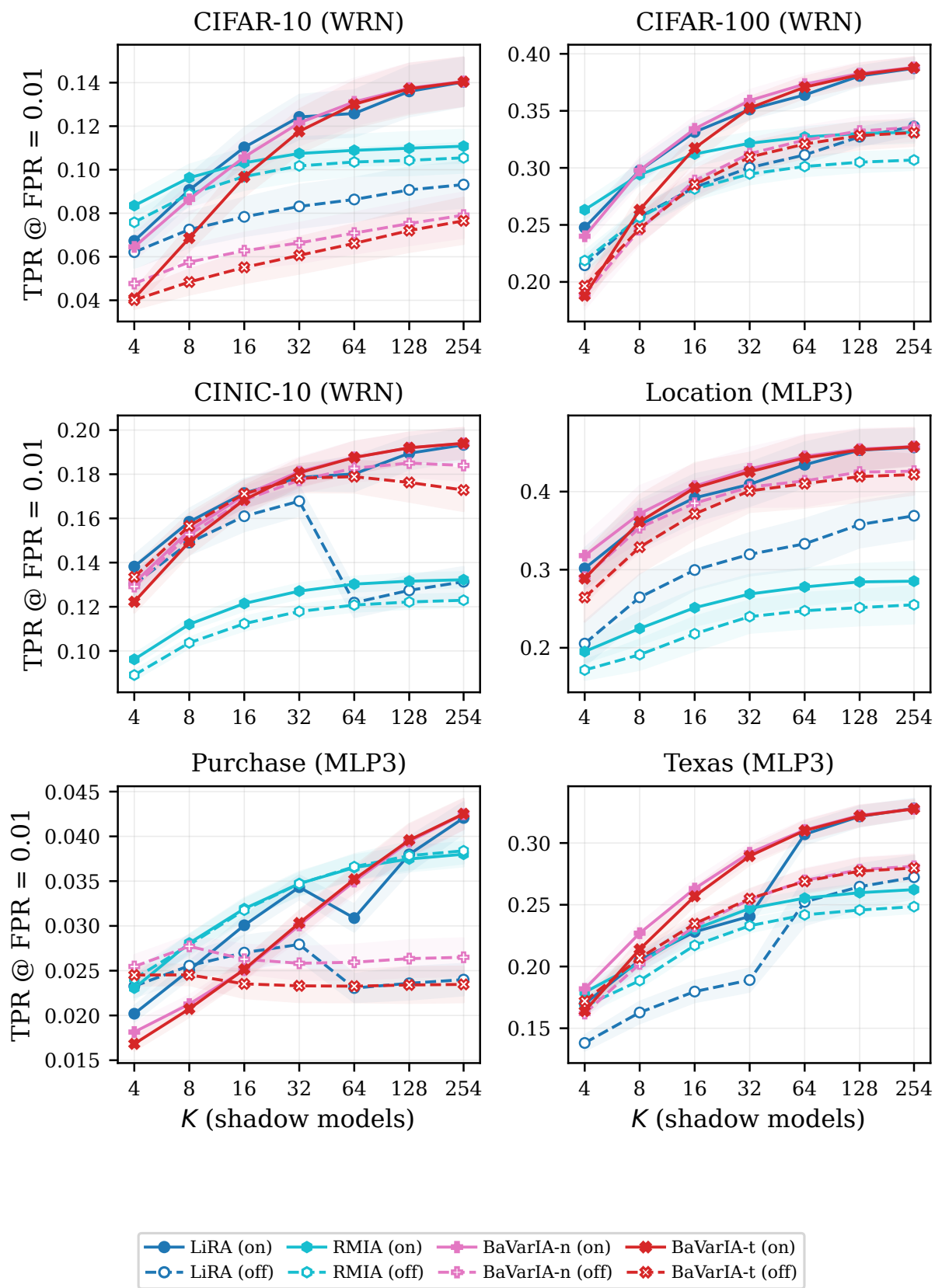


Figure 11: Online vs. offline TPR at FPR=0.01 as a function of K (WRN/MLP3 testbeds). Solid = online, dashed = offline.

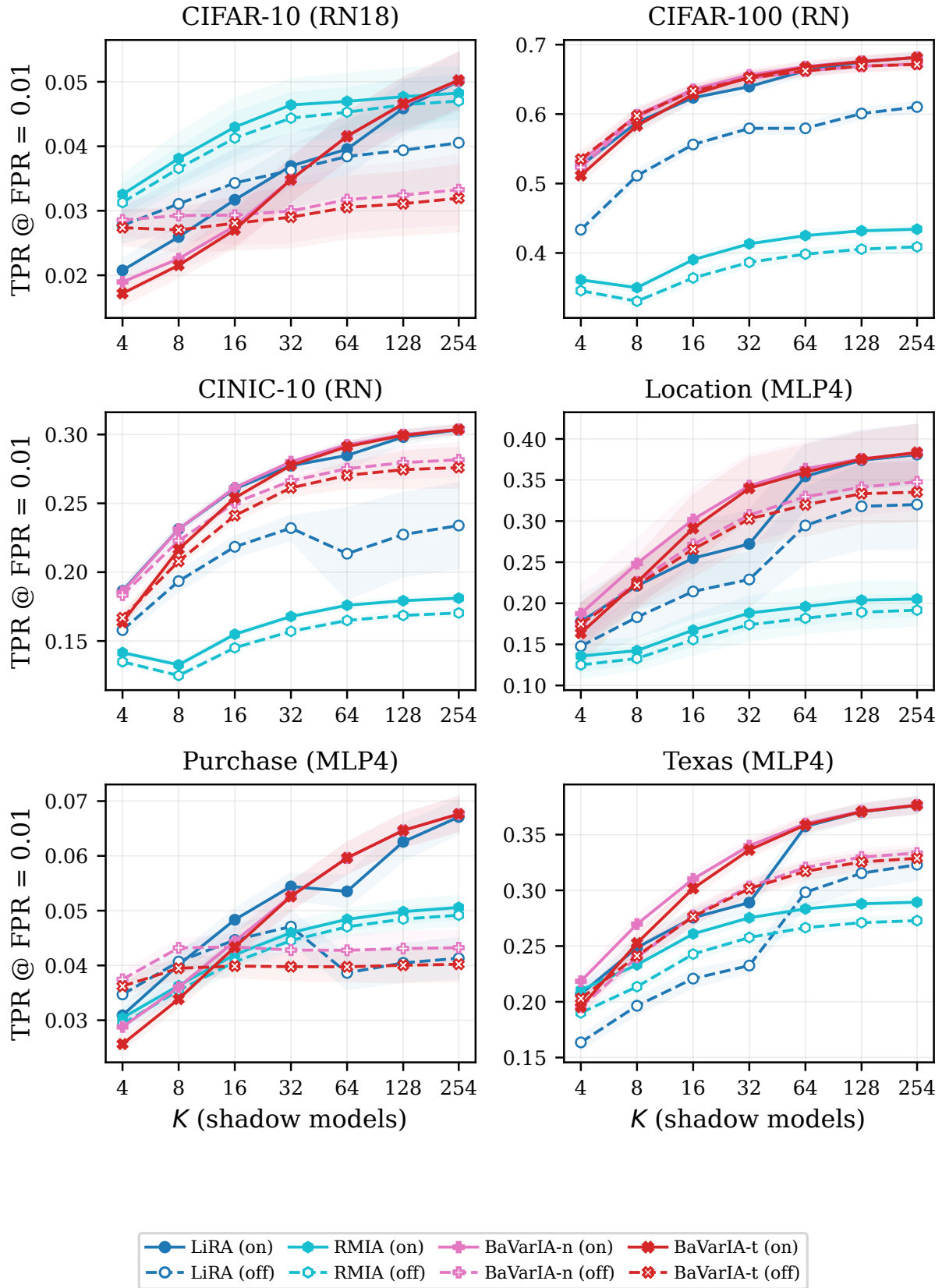


Figure 12: Online vs. offline TPR at FPR=0.01 as a function of K (RN18/MLP4 testbeds).